IZMIR KATIP CELEBI UNIVERSITY
GRADUATE SCHOOL OF NATURAL AND APPLIED SCIENCES

COMPARISON OF TURBULENCE MODELS FOR SINGLE AND MULTIPHASE FLOWS

M.Sc. THESIS

Pelin İLKER

Department of Civil Engineering

Thesis Advisor: Prof. Dr. Mehmet SORGUN

JULY 2020

P. İLKER
IZMIR KATIP CELEBI UNIVERSITY
2020

IZMIR KATIP CELEBI UNIVERSITY
GRADUATE SCHOOL OF NATURAL AND APPLIED SCIENCES

COMPARISON OF TURBULENCE MODELS FOR SINGLE AND MULTIPHASE FLOWS

M.Sc. THESIS

Pelin İLKER
(Y180227008)
ORCID ID 0000-0001-7933-4772

Department of Civil Engineering

Thesis Advisor: Prof. Dr. Mehmet SORGUN

JULY 2020

İZMİR KATİP CELEBİ ÜNİVERSİTESİ
FEN BİLİMLERİ ENSTİTÜSÜ

TEK VE ÇOK FAZLI AKIŞLAR İÇİN TÜRBÜLANS MODELLERİNİN KARŞILAŞTIRILMASI

YÜKSEK LİSANS TEZİ

Pelin İLKER
(Y180227008)
ORCID ID 0000-0001-7933-4772

İnşaat Mühendisliği Ana Bilim Dalı

Tez Danışmanı: Prof. Dr. Mehmet SORGUN

TEMMUZ 2020

Pelin İLKER, a **M.Sc.** student of **IKCU Graduate School Of Natural And Applied Sciences**, successfully defended the thesis entitled " **COMPARISON OF TURBULENCE MODELS FOR SINGLE AND MULTIPAHSE FLOWS**", which he/she prepared after fulfilling the requirements specified in the associated legislations, before the jury whose signatures are below.

Thesis Advisor :

Prof. Dr. Mehmet SORGUN .....
İzmir Kâtip Çelebi University

Jury Members :

Doç. Dr. Gökçen BOMBAR .....
İzmir Kâtip Çelebi University

Doç. Dr. Ali GÜL .....
Dokuz Eylül University

Date of Defense : 24.07.2020

To my family

FOREWORD

I would like to express my sincere gratitude to my thesis advisor Prof. Dr. Mehmet SORGUN who proposed this thesis topic and I started this study under his supervision. I would like to thank him for his guidance, support and encouragement throughout the preparation of this thesis.

I would also like to thank Assoc. Prof. Dr. Gökçen BOMBAR and Assoc. Prof. Dr. Ali GÜL for their valuable advises for this study.

I am grateful to my family, my relatives and my friends for their endless support.

July 2020

Pelin İLKER

TABLE OF CONTENTS

Page

FOREWORD ..... **vi**
TABLE OF CONTENTS ..... **vii**
LIST OF TABLES ..... **viii**
LIST OF FIGURES ..... **ix**
ABBREVIATIONS ..... **x**
ABSTRACT ..... **xi**
ÖZET ..... **xii**
1. INTRODUCTION **1**
1.1 Description of the Problem 1
1.2 Literature Review 2
1.2.1 Turbulent Flow Through Rough Pipes 2
1.2.2 Annular Flow 5
1.2.3 Sediment Transport 9
1.3 Scope of the Study 13
2. THEORY **15**
2.1 Single-Phase Flow 15
2.2 Sediment Transport 16
2.3 Turbulence Models Used In This Study 17
2.3.1 Eddy Viscosity Turbulence Models 18
2.3.1.1 The κ-ε model 20
2.3.1.2 The RNG κ-ε model 21
2.3.1.3 The κ-ω model 21
2.3.1.4 The Shear Stress Transport (SST) Model 22
2.3.2 Reynolds Stress Turbulence Models 22
2.3.2.1 ω -Based Reynolds Stress Model 23
2.3.3 The κ-ε Explicit Algebraic Reynolds Stress (EARSM) Model 23
3. COMPUTATIONAL FLUID DYNAMICS SIMULATION **26**
3.1 Computational Method 26
4. EXPERIMENTAL SETUP **33**
5. RESULTS AND DISCUSSION **38**
5.1 Water Flow Through The Rough Pipe 38
5.2 The Annular Flow 41
5.2.1 Water Flow Through The Eccentric Annulus Including Temperature Effect 41
5.2.2 Water Flow Through The Concentric Annulus 45
5.2.3 Sediment Transport In The Eccentric Annulus 46
6. CONCLUSIONS **50**
REFERENCES **52**
CURRICULUM VITAE **57**

LIST OF TABLES

Page

Table 3.1 Thermal Conditions of Water 30
Table 4.1 Test parameter values during the experiments, rough pipe 34
Table 4.2 Test parameter values during the experiments, water flow in eccentric annulus 35
Table 4.3 Test parameter values during the experiments, water flow in the concentric annulus 36
Table 4.4 Test parameter values during the experiments, the eccentric annulus, sediment transport 37
Table 5.1 Performance comparison of turbulence models based on AAPE, 80 mm pipe diameter 40
Table 5.2 Performance comparison of turbulence models on AAPE, 90 mm pipe diameter 41
Table 5.3 Performance comparison of turbulence models based on AAPE, eccentric annulus 45
Table 5.4 Performance comparison of turbulence models based on AAPE, concentric annulus 46
Table 5.5 Performance comparison of turbulence models based on AAPE, sediment transport 47

LIST OF FIGURES

Page

Figure 1.1 Representative Concentric, Partially Eccentric and Fully Eccentric Annulus [39] 6
Figure 3.1 Flow Chart of the ANSYS CFX 26
Figure 3.2 Rough pipe geometry generation in ANSYS 27
Figure 3.3 Concentric annulus computational mesh 28
Figure 3.4 Concentric annulus geometry 28
Figure 3.5 Determination of optimum mesh for the concentric annulus 29
Figure 3.6 Implementation of the inlet boundary condition 30
Figure 3.7 Implementation of the outlet boundary condition 31
Figure 3.8 Running process of the problem 31
Figure 3.9 Pressure distribution in eccentric annulus 32
Figure 4.1 Izmir Katip Celebi University Civil Engineering Department Flow Loop, rough pipe 33
Figure 4.2 Izmir Katip Celebi University Civil Engineering Department Flow Loop, eccentric annulus 34
Figure 4.3 Middle East Technical University Petroleum Engineering Department Flow Loop, annular test section 36
Figure 5.1 Measured versus calculated pressure gradient (Pa/m), 80 mm rough pipe 39
Figure 5.2 Measured versus calculated pressure gradient (Pa/m), 90 mm pipe diameter 40
Figure 5.3 Measured versus calculated pressure gradient (Pa/m), eccentric annulus, T=25°C 42
Figure 5.4 Measured versus calculated pressure gradient (Pa/m), eccentric annulus, T=40°C 42
Figure 5.5 Measured versus calculated pressure gradient (Pa/m), eccentric annulus, T=50°C 43
Figure 5.6 Measured versus calculated pressure gradient (Pa/m), eccentric annulus, T=60°C 44
Figure 5.7 Measured versus calculated pressure gradient (Pa/m), concentric annulus 46
Figure 5.8 Measured versus calculated pressure gradient (Pa/m), sediment transport 47
Figure 5.9 Simulation of the sediment transport in the eccentric annulus 48
Figure 5.10 Velocity contour plot of sediment transport, v=2.1 m/s 48
Figure 5.11 Velocity contour plot of sediment transport, v=4.2 m/s 49

ABBREVIATIONS

CFD : Computational Fluid Dynamics

3D : Three Dimensional

HAD : Hesaplamalı Akışkanlar Dinamiği

STM : Statistical Turbulence Modeling

LES : Large Eddy Simulation

DNS : Direct Numerical Simulation

RANS : Reynolds-averaged Navier-Stokes

RSM : Reynolds Stress Models

ASM : Algebraic Slip Mixture

DHLLDV : Delft Head Loss& Limit Deposit Velocity

ANN : Artificial Neural Network

GEP : Gene- Expression Programming

ANFIS : Adaptive Neuro-Fuzzy Inference System

SST : Shear Stress Transport

EARSM : Explicit Algebraic Reynolds Stress Model

AAPE : Average Absolute Percentage Error

COMPARISON OF TURBULENCE MODELS FOR SINGLE AND MULTIPHASE FLOWS

ABSTRACT

In hydraulic engineering, the majority of the flow regimes are turbulent. Therefore, understanding and analyzing the turbulence mechanism are of great importance. One of the most commonly used methods in the analysis of turbulence is modeling. Herein, choosing the correct turbulence model is an essential consideration. This study aims to examine the performance of various turbulence models and to understand the turbulence mechanism of the single-phase liquid flow and sediment transport in pressurized pipe systems. For this purpose, six turbulence models mostly used in literature are comparatively investigated. Extensive computational fluid dynamics (CFD) simulations and experimental analysis of water flow in the rough pipe, eccentric and concentric annulus and sediment transport in the eccentric annulus are presented.

The three-dimensional (3D) model is developed by using the computational fluid dynamics (CFD) software, initial and boundary conditions are implemented considering experimental data. Wide range of simulations is performed for flow rates from 16 to 90 m^3/h in the rough pipe, from 6.9 to 31.4 and m^3/h under various temperature conditions in the eccentric annulus, from 6.1 to 26.6 m^3/h in the concentric annulus and the sediment transport in the eccentric annulus for flow rates from 6.1 to 15.9 m^3/h, rate of penetrations from 0.0013 to 0.0101 m/s. The accuracy of turbulent models is verified with the experiments which have been conducted at Izmir Katip Celebi University, Civil Engineering Flow Loop, and presented data by Sorgun [1] and Sorgun and Ulker [2].

Appropriate agreements are obtained between CFD simulations and experiments. It is understood from the results that all models, notably the RNG κ-ε model, can reliably predict the pressure loss for flow through the rough pipe. For the flow through the concentric annulus, the EARSM model outperforms the other turbulence models. Concerning the flow through the eccentric annulus, the RNG κ-ε model performs well at low temperatures, but with decreasing accuracy as the temperature rises. ω-Re turbulence model predicted pressure gradient better than other models at high fluid temperatures. For the sediment transport analysis in closed conduits, all models are observed to yield similar results. However, the κ-ω turbulence model shows slightly better performance when compared to other turbulence models.

Keywords: turbulence models, cfd, annular flow, sediment transport, rough pipe

TEK VE ÇOK FAZLI AKIŞLAR İÇİN TÜRBÜLANS MODELLERİNİN KARŞILAŞTIRILMASI

ÖZET

Hidrolik mühendisliğinde, çoğu akış rejimi türbülanslıdır. Bu nedenle, türbülans mekanizmasını anlamak ve analiz etmek büyük önem taşımaktadır. Türbülans analizinde en sık kullanılan yöntemlerden biri modellemedir. Bu noktada, doğru türbülans modelini seçmek önemli bir husustur. Bu çalışma, çeşitli türbülans modellerinin performansını incelemeyi ve basınçlı boru sistemlerinde tek fazlı sıvı akışı ve sediment taşınımının türbülans mekanizmasını anlamayı amaçlamaktadır. Bu amaçla, literatürde en çok kullanılan yedi türbülans modeli karşılaştırmalı olarak incelenmiştir. Hesaplamalı akışkanlar dinamiği (HAD) simülasyonları ve pürüzlü borudaki su akışı, eksantrik ve eşmerkezli iç içe iki boruda su akışı ve eksantrik iç içe iki boruda sediment taşınımının deneysel analizi kapsamlı bir biçimde sunulmaktadır.

Üç boyutlu model, hesaplamalı akışkanlar dinamiği (HAD) yazılımı kullanılarak geliştirilmiş, deneysel veriler dikkate alınarak başlangıç ve sınır koşulları uygulanmıştır. Debi değerleri, pürüzlü boruda 16 ila 90 m^3/sa, eksantrik iç içe iki boruda çeşitli sıcaklık koşullarında 6.9 ila 31.4 m^3/sa, eşmerkezli iç içe iki boruda 6.1 ila 26.6 m^3/sa olmak üzere ve eksantrik iç içe iki boruda sediment taşınımı için ise debi değerleri 6.1 ila 15.9 m^3/sa, penetrasyon hızları 0.0013 ila 0.0101 m/s olmak üzere çok sayıda simülasyon gerçekleştirilmiştir. Türbülans modellerinin doğruluğu, İzmir Katip Çelebi Üniversitesi İnşaat Mühendisliği Bölümü deney düzeneğinde yapılan deney verileri ve Sorgun [1] ve Sorgun ve Ulker'in [2] verileri kullanılarak saptanmıştır.

HAD simülasyonları ve deney sonuçlarının birbirleriyle uyum içinde olduğu görülmüştür. Sonuçlardan anlaşılacağı üzere, başta RNG κ-ε modeli olmak üzere tüm modeller, pürüzlü boruda akış için basınç kaybını güvenilir bir şekilde tahmin edebilmektedir. Eş merkezli iç içe iki boru arasından akış için, EARSM modeli diğer türbülans modellerinden daha iyi performans göstermiştir. Eksantrik iç içe iki boru arasından akış durumunda, RNG κ-ε modeli düşük sıcaklıklarda iyi performans göstermektedir. Bununla beraber akışkanın sıcaklığı arttıkça tüm türbülans modellerinin basınç farkını tahmin etme performansları kötüleşmektedir. ω-Re türbülans modeli, yüksek sıcaklıklarda basınç gradyanını diğer modellerden daha iyi tahmin etmiştir. Boruda sediment taşınımı analizinde ise, tüm modellerin benzer sonuçlar verdiği gözlemlenmiştir. Ancak, κ-ω türbülans modeli, diğer türbülans modelleriyle karşılaştırıldığında biraz daha iyi performans göstermektedir.

Anahtar kelimeler: türbülans modeli, had, iç içe iki boru arasından akış, sediment taşınımı, pürüzlü boru

1. INTRODUCTION

1.1 Description of the Problem

Turbulent flows are handled by engineering, physics, and earth sciences where moving fluids such as volumes of water or air are studied. Turbulence is observed in almost all flows from large scale processes such as oceanic currents or atmospheric flow of air to small scale problems such as the efficiency of a wind turbine or wind loads over structures [3].

Turbulent flow is the most complex type of fluid flow that makes its exact definition difficult. It has properties that complicate the turbulence process, including efficient mixing, irregularity in time and space, nonlinearity, large Reynolds numbers, dissipation, continuous spectra of length and time scales. Modeling of turbulence with various approaches results from that the turbulence process cannot be calculated by an exact method. To obtain reasonable engineering simulations of turbulent flows, the understanding of how turbulence models are developed, choosing, and correctly implementing these models is needed.

Turbulent flow is described by Navier-Stokes equations that cannot be solved with an exact method and the numerical strategies are available to solve these equations. As a basis, there are three methods used for the prediction of turbulent flow which are; statistical turbulence modeling (STM), large eddy simulation (LES), and direct numerical simulation (DNS) [4-7]. Since the Direct Numerical Simulation (DNS) of turbulent flow requires considerable computational effort, many CFD studies have been focused on statistical turbulence modeling to investigate the effects of turbulence [8].

In most engineering applications, working with the mean flow field is sufficient. The purpose of predicting turbulent flows for design and analysis is to calculate the related physical conditions by using the simplest and the most economical mathematical model possible. The prediction of turbulent flows should be accurate as well as

computationally economical. For that reason, turbulence modeling not only provides meaningful results but also saves a huge amount of money and time by avoiding the experimental work costs and choosing the proper model [9,10].

Attempts to define turbulence and related systematic studies date back to the nineteenth century. Initial studies to predict the effects of turbulence were conducted by empirical formulas through one-dimensional analytical approaches. Later, numerical solutions have been introduced for more complex multidimensional differential equations that govern turbulence with the development of computer technology. Statistical turbulence models that use Reynolds-averaged Navier-Stokes (RANS) equations, Direct Numerical Simulation (DNS) that can solve original time-dependent Navier-Stokes equations and Large Eddy Simulation (LES) in which the turbulent motion is analyzed only to the scale of the numerical grid and the fluctuating motion of the scale smaller than the mesh size is modeled by a subgrid-scale model were developed to investigate the turbulence effects [11].

Consequently, although extensive studies have been developed for many years, turbulence modeling remains one of the major concerns of the fluid engineering field. Therefore, further experimental and numerical studies are of great importance in understanding the turbulence mechanism and determination of the performance of turbulence models.

1.2 Literature Review

1.2.1 Turbulent Flow Through Rough Pipes

Many engineering systems such as re-entry vehicles, missiles, aircraft, ships, turbines, heat exchangers, piping networks, and atmospheric flows have rough surfaces aerodynamically. Thus, modeling turbulent flow over rough surfaces accurately is a substantial concern [12].

The basis for the work on turbulent flows over rough walls is laid by Hagen [13] and Darcy [14] who studied pressure losses in closed conduits [15]. One of the most important contributions in this regard was made by Nikuradse [16] with his work on equivalent sand roughness which influences the flow structure in the near-wall region.

He conducted extensive measurements of the pressure drop and the flow rate to calculate the friction factor and presented the equation for the case of rough pipe flow:

$$\frac{1}{\sqrt{f}} = -2.0 \log\left(\frac{D}{\varepsilon}\right) + 1.74 \tag{1.1}$$

Colebrook [17] collected results for several industrial pipes and suggested an implicit formula of friction factor for turbulent flow in smooth as well as rough pipes:

$$\frac{1}{\sqrt{f}} = -2.0 \log\left(\frac{\varepsilon/D}{3.7} + \frac{2.51}{Re\sqrt{f}}\right) \tag{1.2}$$

where f is friction factor, ε/D is relative roughness and Re is Reynolds number. Moody [18] later presents a diagram named Moody chart which presents the Darcy friction factor for pipe flow as a function of Reynolds number and ε/D [19].

Perry et al. [20] revealed an experimental study of turbulent boundary layer development over rough walls. They worked with two types of wall roughness geometries each has different law of behavior. They stated that the roughness represented by the grooves in the wall is a function of the length of scale and does not compromise the Nikuradse-Clauser correlation scheme. Their results showed that the length of the scale is probably proportional to the boundary layer thickness for zero pressure gradient condition.

Shockling et al. [21] studied on the fully developed turbulent pipe flow that shows hydraulically smooth, transitionally rough, and fully rough behaviors. They concluded that the friction factor in the transitionally rough regime, this surface follows a Nikuradse [16]-type inflectional relationship rather than the Colebrook [17] relationship used in the Moody diagram. The velocity profiles in outer scaling were in good agreement with Townsend's [22] hypothesis and the magnitude of the downward shift in the velocity profile showed transitional behavior qualitatively similar to sand-grain roughness in contrast with Colebrook. A similar study using a different range of Reynolds numbers was presented by Allen et al [23]. In addition to the identical results, they expressed that the transitional friction factor curves for honed pipes of arbitrary relative roughness were developed by using the size of the velocity shift versus roughness Reynolds number data and the inflection in the transitional regime remained

constant while surface geometry changed in support with the model of Gioia and Chakraborty [24].

The experimental study was conducted by Hultmark et al. [25] that presents the measurements of the streamwise component of the velocity in fully developed pipe flow for different roughness conditions. They investigated the logarithmic behavior of the streamwise Reynolds stress under hydraulically smooth, transitionally rough, and fully rough cases.

Patel [26] presented a review of principal results of common experiments on the effects of sand grain roughness and several models for considering these effects in numerical solutions. He also emphasized the importance of proving the accuracy of CFD models by comparing them with the experimental data and the necessity of related future studies.

A numerical analysis based on the effect of surface roughness and heat transfer characteristics in laminar flow was performed by Ibrahim et al. [27] They used the commercial CFD software to examine different roughness values and the variation of heat transfer and fluid characteristics with the increase in roughness. They compared the results with the analytical solution and experimental data from the literature. They stated that the pressure drop increased with increasing surface roughness matching the data available in the literature.

Hellsten and Laine [28] proposed an enhanced computational method to estimate the behavior of turbulent flows over rough surfaces regarding the numerical solution of the Navier-Stokes equations employing the κ-ω-SST turbulence model for rough flat-plate flows and flows past a rough aerofoil. They obtained good results for flat-plate flows when compared the calculated velocity profiles and skin-friction distribution with experimental data and in producing the effect of roughness on the lift and drag the aerofoil section.

Vijiapurapu and Cui [29] investigated the performance of the turbulence models and discussed the outperforming techniques for the fully developed turbulent flow in circular roughened pipes. They solved the Reynolds-averaged Navier–Stokes (RANS) equations with turbulence models which are κ-ε, κ-ω, Reynolds stress models (RSM), and filtered Navier–Stokes equations with Large Eddy Simulation (LES). The

accuracy of numerical results was confirmed with the experimental measurements presented by Nourmohammadi et al. [30] and other numerical data published in the literature [31,32].

Huang et al. [33] examined the friction factor in rough pipes with large surface roughness both experimentally and analytically. They found that the Reynolds number between flow regimes decreased as the relative roughness increased. The range of Reynolds number for the transitional flow regime decreased as the surface roughness increased. They also experienced that the approaches applied for laminar flow did not correspond to turbulent flow.

Szilas et al. [34] studied on the analysis of the turbulent pressure loss of Non-Newtonian fluid flow in rough pipes both analytically and experimentally. They offered a friction factor formula for the turbulent flow of power-law type fluids in the transition region. They also conducted a set of experiments to verify the accuracy of their formula. They indicated that the calculated data were in accordance with the measured data. Similar studies were revealed by many researchers. Shaikh et al. [35] and Brkic [36] proposed an explicit approximation to Colebrook's friction factor in rough pipes for turbulent flows.

Avci and Karagöz [37] derived a single explicit equation for laminar, transition, and turbulent flows in smooth and rough pipes. They validated the accuracy of the formula by the Colebrook's equation and experimental data from the literature. They stated that the equation provided an accurate and quick solution for the friction factor which is used for the calculation of pressure loss.

1.2.2 Annular Flow

Annular flow is described as the flow of fluid in the gap between two pipes. There has been considerable interest for long years in flow and heat transfer problems in annuli, both concentric and eccentric. Therefore, it is of high importance to analyze the annular flow properly. The annulus can be defined as the space between two cylinders, one of which located inside the other. The definition of the eccentricity is as follows:

$$e = \frac{\delta}{(r_o - r_i)} \tag{1.3}$$

where δ is offset distance between the center of inner and outer pipes, r_i is outer radius of inner pipe r_o is inner radius of outer pipe. For concentric annuli, e=0, while for a fully eccentric annuli, e=1 [38,39]. The annular geometries considered in the present study is shown in Figure 1.1.

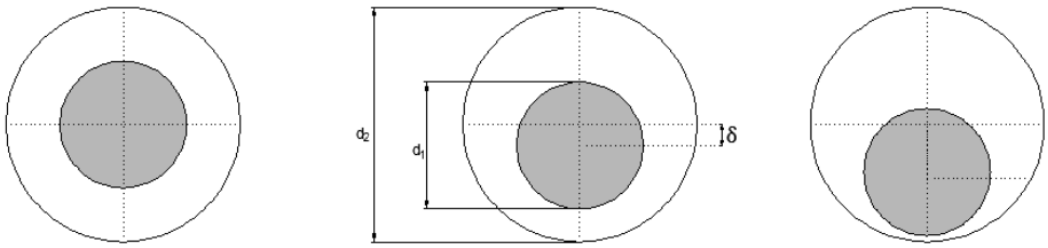

Figure 1.1 Representative Concentric, Partially Eccentric and Fully Eccentric Annulus [39].

Since the annular turbulent flow is part of the many engineering applications such as heat exchangers, nuclear reactor cores, combustion systems, investigation of this concern is highly important [40].

The numerical and experimental studies were performed by Erge et al. [41] to predict the annular frictional pressure losses with and without pipe rotation for the flow of Newtonian and non-Newtonian fluids in annuli. They presented a finite difference model and it was validated with CFD software. The results obtained from the numerical model offers a good compromise with the experiments and the experimental data from the literature. They stated that the performance of the proposed model is better than the existing methods.

Sorgun and Ozbayoglu [42] carried out an extensive study to investigate the non-Newtonian fluids flow through both horizontal concentric and eccentric annulus. The experiments were conducted and frictional pressure losses were estimated by using an Eulerian-Eulerian computational fluid dynamics (CFD) model. They observed that the CFD model results and the experimental data were in good agreement.

Haciislamoglu and Langlinais [43] conducted a numerical study on the laminar flow of Non-Newtonian fluids by using a finite differences technique to obtain velocity and viscosity profiles and flow rate. The numerical model was verified with the experimental data from the literature. They remarked that the frictional pressure losses

were decreased with an increasing eccentricity for a constant flow rate. They found out a correlation for a quick prediction of frictional pressure losses of power-law fluids in an eccentric annulus.

A numerical and experimental study of laminar, transitional, and turbulent non-Newtonian flow in skewed narrow annular and uniformly eccentric geometries were presented by Haciislamoglu and Cartalos [44]. They developed a method that can be used in all annular pressure loss calculations.

Kelessidis et al. [45] carried out an experimental study to predict the pressure losses of fluids in concentric and fully eccentric annuli in laminar, transitional, and turbulent flow regimes. They compared the results from the experiments with the model results presented formerly for concentric annulus and achieved good agreement. They also obtained significant results for the eccentric annulus by correcting the eccentricity with the correlations of Haciislamoglou et al. [43,44]

Sorgun [46] investigated the pipe eccentricity effect on frictional pressure loss, tangential velocity, axial velocity, and effective viscosity of water and non-Newtonian fluids for concentric, partially eccentric, and fully eccentric annuli by using computational fluid dynamic software. He validated the estimated pressure losses with experimental data in addition to the basic theoretical calculations. He observed that the estimated pressure drop values gave good results when compared to experimental data almost for all cases.

Sayindla et al. [47] studied on the hydraulics of non-Newtonian fluid flow in an eccentric annulus with pipe rotation by using computational fluid dynamics (CFD). They also conducted a set of experiments and they obtained good agreement when the results were comparatively examined. They reported that the pressure drop increases with the pipe rotation and the frictional pressure losses increased as the density and viscosity values got higher.

Uner et al. [48] proposed an approximate solution that represented the relationship between the volume rate of flow and pressure drop as a function of eccentricity and radius ratios. They expressed that the model is convenient for larger radius ratios in an eccentric annulus.

Luo and Peden [49] suggested a new model for the investigation of fluid flow through eccentric annuli. They obtained analytical solutions for the shear stress, shear rate, velocity, and volumetric flow rate/pressure gradient for Non-Newtonian fluids. They indicated that the model could be simply applied and gave good results. They also added that the turbulent flow in eccentric annulus showed similar behavior to those found in the laminar flow.

Brighton and Jones [50] presented the measurements of the mean-velocity distributions and the location of the maximum mean velocity for various flow conditions in the concentric annulus. It was emphasized that the point of maximum mean velocity in turbulent flow occurred at a smaller radius than in laminar flow, the mixing length and eddy-viscosity distributions were very large at the maximum velocity region. Quarmby [51] also achieved complementary results with a similar experimental study.

Rehme [52] conducted an experimental analysis to measure the pressure drop, the positions of zero shear stress and maximum velocity, and the velocity distribution in concentric annuli. He discovered that the position of zero shear stress did not overlap the position of maximum velocity contrary to common opinion.

Levy [53] found out the derivation of equations defining fully developed turbulent flow in an annulus to predict the location of the plane of zero shear, mixing length, eddy diffusivity, velocity distribution, and friction factor.

Singh et al. [54] carried out the theoretical study about the developing and fully developed turbulent flow of Newtonian fluid through a concentric annulus and verified with the experimental data. The equation for the entrance region was extended to turbulent flow through the annulus was linearised by the technique from the literature and cohered with the experimental data. They also concluded that the stress in the inner region is higher than that in the outer region and the energy loss per unit volume is higher in the inner region due to higher turbulence.

An extensive experimental study on the flow of the Newtonian and Non-Newtonian fluids in concentric and eccentric annuli was presented by Nouri et al. [55] They stated that the Newtonian fluid flow was in the concentric annulus as expected and in eccentric annulus circumferential variation of the maximum axial velocity was

observed. The skin friction coefficient of the Newtonian fluid varied with the Reynolds number demonstrated that the flow resistance increased in the concentric annulus and decreased in the eccentric annulus when compared to smooth pipe flow.

Sorgun et al. [56] recommended a mechanistic model to estimate the frictional pressure losses of light drilling fluid in concentric annuli for both laminar and turbulent flow. To affirm the accuracy of the model, the experimental data available in the literature, and the computational fluid dynamics (CFD) software were used. Results showed that the predictions of the frictional pressure losses were in acceptable error intervals.

Xiong et al. [57] carried out a computational fluid dynamics (CFD) simulation to investigate the near-wall turbulent structures for fully turbulent flow in the concentric annuli by using the Reynolds-Averaged Navier–Stokes (RANS) model. The CFD results were compared to the experimental data available in the literature. They observed that the model was able to predict the asymmetric features of turbulent flows in the annulus. They also compared the results from the RANS model with those from the direct numerical simulation (DNS) from the literature.

1.2.3 Sediment Transport

The sediment transportation with carrying fluid through pipelines is seen in various industrial operations such as dredging, construction of dams, design of storm sewers, processing plants, coal transportation to thermal power plants, transportation of waste materials [58,59].

The two-phase solid-liquid flow in the horizontal pipeline by using computational fluid dynamics (CFD) software was modeled by Singh et al. [59]. They obtained the pressure drop values for various solid concentrations and velocities. The simulation results and the experimental data existing in the literature were in good agreement.

Kökpınar and Göğüş [60] developed a new empirical correlation to predict the critical flow velocity of sediment transport in horizontal pipelines. They conducted experimental and theoretical studies. They found the accuracy of the empirical correlation was adequate when compared with the observed data. It was concluded that the proposed equation was suitable for the noncohesive, uniform, and nonuniform coarse particles reliably.

Ling et al. [61] investigated the sand-water slurry flow numerically by using a 3D algebraic slip mixture (ASM) method with RNG κ-ε turbulence model. They obtained significant results when compared to the calculated data with the measured data and also made some important contributions to the slurry flow characteristics.

Amanna and Movaghar [62] carried out a study on the sediment transport behavior and the affecting parameters. They performed the experimental study and the simulation by using computational fluid dynamics (CFD). The measured and calculated data gave appropriate results. An empirical correlation was developed to predict the cutting concentration by using the Buckingham- π theorem.

Kaushal et al. [63] investigated the pipeline flow of fine particles at the high concentration by using Mixture and Eulerian two-phase models to predict the pressure drop, concentration distribution, velocity distribution, shear stress distribution, vertical velocity distribution, and granular viscosity and pressure distributions. They compared the data predicted by the numerical model with the experimental data obtained from the previous work of the author. It was stated that the Eulerian method gave good results for pressure drop and concentration distribution.

A steady-state three-layer mechanistic model for solid-liquid flow to predict the pressure loss, critical velocity, and concentration profiles was presented by Shirazi and Frigaard [64]. They also developed a correlation for the turbulent solids diffusivity. When compared the predicted data obtained from the steady-state model and the new correlation with the experimental data available in the literature, the convenient results were obtained.

An empirical equation for frictional pressure losses and cuttings bed thickness was proposed by Sorgun [65]. The precision of the empirical equation was verified experimentally. The experiments were performed for various parameters, such as hole inclination, flow velocities, rate of penetration, and pipe rotation with water and non-Newtonian fluids. It can be inferred that the empirical correlations were effective for the field studies.

Ting et al. [66] examined the behavior of the fully- suspended slurry flow in the horizontal pipeline. They used the Computational Fluid Dynamics (CFD) model and the Delft Head Loss& Limit Deposit Velocity (DHLLDV) method to predict the

hydraulic gradient and concentration distribution. They compared the results obtained from the models with the experimental data from the literature and obtained very good agreement.

Lahiri and Ghanta [67] proposed a correlation to estimate the hold-up of sediment transport in pipelines. They used the Artificial Neural Network (ANN) method to derive the correlation depending on the measurements available in the literature. They reported that the ANN correlation predictions were satisfactory when compared with the correlations from the literature.

The critical velocity as a design parameter in sediment transport systems to prevent the clogging of the pipeline was investigated by Azamathulla and Ahmad [68] by using Gene- expression programming (GEP) and Adaptive neuro-fuzzy inference system (ANFIS) techniques and they compared the GEP and ANFIS results with the empirical data existed in the literature. It was concluded that the models gave better results than the existing formula in the literature. They also developed a formula with the GEP model for the estimation of the critical velocity. They obtained significant results when compared with the existing data.

An experimental study focused on the two-phase flow was carried out by Alizadehdakhel et al. [69] conducted and the pressure drop values were estimated by using CFD and ANN methods. When compared the results of the CFD and ANN with the experimental outputs, it was observed that the CFD model predictions were more reliable.

Ulker and Sorgun [70] conducted a study on the prediction of the cuttings bed thickness inside a wellbore with and without pipe rotation. The k- Nearest Neighbor (kNN), Support Vector Regression (SVR), Linear Regression and Artificial Neural Network (ANN) methods were carried out as a computational intelligence techniques to predict the cuttings bed thickness. The experiments were performed for various parameters. When compared the calculated data with the measured data, the remarkable results were obtained. The ANN method gave more precise results than the other models, whereas the kNN method was more timesaving.

Capecelatro and Desjardins [71] analyzed the slurry flow behavior in the horizontal pipes under the above and the below critical velocity conditions by using the Large

Eddy Simulation (LES) method associated with a Lagrangian particle tracking solver. The substantial results were obtained from the simulation when compared with the experimental data from the literature.

Messa and Malavasi [72] simulated the fully- suspended solid-liquid slurry flow in a horizontal pipeline and they reported that the accuracy of the pressure gradient was developed.

Cao and Chiew [73] conducted an experimental study and simulated the system by CFD. They observed the suction effects on sediment transport in closed conduits and obtained good results.

Arolla and Desjardins [74] presented the numerical simulations to investigate the mechanism of turbulent liquid-solid slurry flow by using a volume-filtered Euler-Lagrange large eddy simulation method. Numerical simulations identified the mean velocity, mean concentration, and mean pressure gradient. They obtained good results when compared to the simulation results with the experimental data available in the literature.

Zhang et al. [75] conducted both analytical and numerical studies to investigate the grouting mechanism of cement-based slurry in a concentric annulus under high groundwater pressure. They derived the equation of motion for the axial flow of the Newtonian fluid in a long concentric annulus and determined the distribution of pressure and slurry viscosity in the grouted zone, the variations in injection pressure at the grouting point and the grouting flow rate by using the stepwise calculation method and the variations in injection pressure at the grouting point and grouting flow rate. They accessed good results when compared to the results from the stepwise calculation method with those from the numerical work.

Sorgun [76] suggested a mechanistic model to predict the cuttings bed thickness in horizontal and inclined wells by using the finite differences method. The results from the model were compared with those from the experiments and were shown to be in good agreement.

Escudier et al. [77] carried out extensive studies both experimental and numerical. They investigated the fully developed laminar flow of a shear-thinning liquid through concentric and eccentric annulus with and without pipe rotation. They obtained good

results when they compare the results of the experiments with the numerical calculations and the experimental data available in the literature.

Ozbayoglu et al. [78] conducted cuttings transport experiments in horizontal and directional wells. They emphasized the effect of pipe rotation and found that the pipe rotation affected the cuttings transport positively.

Another experimental work in a cuttings transport flow loop was implemented by Sorgun et al. [79] They observed the pressure drop values for variable flow rates, cuttings concentrations, pipe inclinations, and rotation speeds and offered the empirical correlations and charts for friction factor considering low and high viscosity fluids in terms of combined Reynolds number and stationary cuttings bed thickness.

A numerical study on the cuttings transport in a vertical eccentric well was presented by GhasemiKafrudi and Hashemabadi [80], the flow field parameters and the pressure drop was obtained. The results were found to be in accordance with the data from the literature.

Ofei et al. [81] performed a numerical study to predict the pressure drop values for the cuttings-liquid flow in an eccentric horizontal narrow annulus with drillpipe rotation. They examined the effects of diameter ratio, fluid velocity, fluid type, fluid rheology, and drillpipe rotation speed on pressure drop by using CFD. They verified the simulation results with the experimental data from the literature and they observed that the pressure drop increased significantly when the fluid velocity and diameter ratio increased.

Neto et al. [82] also simulated the turbulent flow in concentric and eccentric annuli with and without rotating the inner pipe. They used various turbulence models employed Reynolds Average Navier–Stokes equations and evaluated the results in terms of the velocity profiles. They obtained good results when they compared the simulation results with the experimental data from the literature. They also stated that the standard Reynolds Stress model performed better than the other turbulence models.

1.3 Scope of the Study

This study aims to evaluate the performance of various turbulence models, which are mostly used in literature, for the prediction of the flow behavior and pressure gradients

in the rough pipe and the annulus. Extensive studies were conducted on the water flow through a rough pipe, water flow in the annulus, and slurry flow in annulus under a wide range of conditions. Various flow rates, annular dimensions, and temperature values were carried out in the CFD simulations of those flows. The accuracy of the turbulence models was verified by the experimental data obtained from the previously published literature.

The governing equations and the theoretical information of the turbulence models adopted are referred in Chapter 2. In Chapter 3, computational fluid dynamics simulations are explained in detail. Chapter 4 summarizes the experimental work. The results and discussion are presented in Chapter 5 and the findings of this study are declared in Chapter 6.

2. THEORY

Turbulent flows can be defined completely by the solution of time-dependent three-dimensional Navier-Stokes equations. To enable the effects of turbulence to be predicted, the Reynolds Averaged Navier-Stokes (RANS) equations were introduced including the time-averaged quantities [83].

In this study, turbulent models using RANS equations as a governing equation are analyzed to investigate the effect of turbulence on single and multiphase flows [84].

The assumptions used in the analysis are as follows:

- The fluid is incompressible.
- Steady-state and fully developed flow.
- Isothermal system (physical properties are constant).

2.1 Single-Phase Flow

The Reynolds averaged continuity and momentum equations in conservation form are:

$$\frac{1}{r}\frac{\partial(rv)}{\partial r}+\frac{1}{r}\frac{\partial w}{\partial \theta}+\frac{\partial u}{\partial z}=0 \tag{2.1}$$

$$\frac{\partial u}{\partial t}+\frac{1}{r}\frac{\partial[r(uv)]}{\partial r}+\frac{\partial(uw)}{r\partial\theta}+\frac{\partial(uu)}{\partial z}=-\frac{1}{\rho}\frac{\partial p}{\partial z}-gcos\emptyset+\frac{1}{r}\frac{\partial(r\tau_{rz})}{\partial r}+\frac{1}{r}\frac{\partial(r\tau_{\theta z})}{\partial\theta}+\frac{1}{r}\frac{\partial(r\tau_{zz})}{\partial z}+\frac{1}{r}\frac{\partial[r(\overline{-u'v'})]}{\partial r}+\frac{1}{r}\frac{\partial(\overline{-u'w'})}{\partial\theta}+\frac{\partial(\overline{-u'u'})}{\partial z} \tag{2.2}$$

$$\frac{\partial v}{\partial t}+\frac{1}{r}\frac{\partial[r(vv)]}{\partial r}+\frac{\partial(vw)}{r\partial\theta}+\frac{\partial(vu)}{\partial z}-\frac{ww}{r}=-\frac{1}{\rho}\frac{\partial p}{\partial r}+gsin\emptyset cos\theta+\frac{1}{r}\frac{\partial(r\tau_{rr})}{\partial r}+\frac{1}{r}\frac{\partial(r\tau_{\theta r})}{\partial\theta}+\frac{1}{r}\frac{\partial(r\tau_{zr})}{\partial z}-\frac{\tau_{\theta\theta}}{r}+\frac{1}{r}\frac{\partial[r(\overline{-v'v'})]}{\partial r}+\frac{1}{r}\frac{\partial(\overline{-v'w'})}{\partial\theta}+\frac{\partial(\overline{-v'u'})}{\partial z}-\frac{\overline{-w'w'}}{r} \tag{2.3}$$

$$\frac{\partial w}{\partial t}+\frac{1}{r}\frac{\partial[r(wv)]}{\partial r}+\frac{\partial(ww)}{r\partial\theta}+\frac{\partial(wu)}{\partial z}+\frac{wv}{r}=-\frac{1}{\rho r}\frac{\partial p}{\partial\theta}-gsin\emptyset sin\theta+\frac{1}{r}\frac{\partial(r\tau_{r\theta})}{\partial r}+\frac{1}{r}\frac{\partial(r\tau_{\theta\theta})}{\partial\theta}+\frac{1}{r}\frac{\partial(r\tau_{z\theta})}{\partial z}-\frac{\tau_{r\theta}}{r}+\frac{1}{r}\frac{\partial[r(\overline{-w'v'})]}{\partial r}+\frac{1}{r}\frac{\partial(\overline{-w'w'})}{\partial\theta}+\frac{\partial(\overline{-w'u'})}{\partial z}-\frac{\overline{-w'v'}}{r} \tag{2.4}$$

where u, v, w are the fluid velocities in cylindrical coordinates and, p is the pressure, ρ is the density, τ_{ij} denotes the viscous stress tensor. The RANS (Reynolds Averaged Navier Stokes) equations are obtained by decomposing the dependent variables of the system into mean (indicated with a bar) and fluctuating (indicated with prime) components.

2.2 Sediment Transport

The solid-liquid flow inside horizontal wellbores is modeled by using an Eulerian-Eulerian computational fluid dynamics (CFD) model for various fluid velocities, rates of penetration.

The equation of continuity for both the fluid and solid phase can be written as [85, 86]

$$\frac{\partial}{\partial t}\left(\rho_f C_f\right) + \nabla.\left(\rho_f C_f U_f\right) = 0 \tag{2.5}$$

$$\frac{\partial}{\partial t}\left(\rho_s C_s\right) + \nabla.\left(\rho_s C_s U_s\right) = 0 \tag{2.6}$$

with the constraint

$$C_f + C_s = 1 \tag{2.7}$$

where the subscripts f and s denote, respectively, the fluid and solid phase, C is the mean volume fraction, ρ is density, U is velocity vector, and t is time.

The momentum equation for each phase is expressed as [85-87]

$$\rho_f C_f \left[\frac{\partial U_f}{\partial t} + U_f.\nabla U_f\right] = -C_f \nabla \mathrm{P} + C_f \nabla.\tau_f + C_f \rho_f g - M \tag{2.8}$$

and for the solid phase;

$$\rho_s C_s \left[\frac{\partial U_s}{\partial t} + U_s.\nabla U_s\right] = -C_s \nabla \mathrm{P} + C_s \nabla.\tau_s + C_s \rho_s g - \nabla P_s + M \tag{2.9}$$

where P is pressure, g is the gravitational acceleration vector, τ is the viscous stress tensor, P_s is solid pressure, and M is the interfacial momentum transfer per unit volume made up of the drag force, F_d, and the lift force, F_l.

2.3 Turbulence Models Used In This Study

Turbulence models depending on RANS equations are defined as Statistical Turbulence models which are;

- Zero equation models

These models simply compute the constant eddy viscosity value from the mean velocity and a geometric length scale using an empirical formula for the entire flow domain. The viscous contribution from turbulent eddies is calculated by using an algebraic equation.

- Two equation models

These models compute the velocity and length scale by using separate transport equations and correspondingly the turbulent viscosity is modeled. The turbulence velocity scale is obtained from the turbulent kinetic energy and the turbulent length scale is obtained from the turbulent kinetic energy and its dissipation rate.

- Reynolds stress equation models

These models solve transport equations for the Reynolds stress components separately depending on the Reynolds stress tensor and the dissipation rate.

- Algebraic stress models

These models deal with algebraic equations for the Reynolds stresses.
In this study, the Eddy viscosity models, the Reynolds stress models, and the Algebraic stress models are used.

In the RANS equation, turbulent variables are divided into a time-averaged component and a time-varying fluctuating component. Accordingly, the velocity can be written as:

$$U_i(\mathrm{x, t}) = \overline{U}_i\,(\mathrm{x}) + u'_i(\mathrm{x, t}) \tag{2.10}$$

and the average velocity is,

$$\overline{U}_i = \frac{1}{\Delta t}\int_t^{t+\Delta t} U_i dt \tag{2.11}$$

where Δt is the time scale which is considerably larger than the turbulent fluctuations.

When the decomposition and averaging operations of the velocity are applied to the original Navier–Stokes equations, the continuity equation, and the momentum conservation equation are expressed as:

$$\frac{\partial \rho}{\partial t} + \frac{\partial}{\partial x_j}\left(\rho U_j\right) = 0 \tag{2.12}$$

$$\frac{\partial \rho U_i}{\partial t} + \frac{\partial}{\partial x_j}(\rho U_i U_j) = \frac{\partial p}{\partial x_i} + \frac{\partial}{\partial x_j}\left[\tau_{ij} - \rho\overline{u_i u_j}\right] + S_M \tag{2.13}$$

where τ is the molecular stress tensor and $\rho\overline{u_i u_j}$ is Reynolds stress.

The Reynolds averaged energy equation is:

$$\frac{\partial \rho h_{tot}}{\partial t} - \frac{\partial \rho}{\partial t} + \frac{\partial}{\partial x_j}(\rho U_j h_{tot}) = \frac{\partial}{\partial x_j}\left(\lambda \frac{\partial T}{\partial x_j} - \rho\overline{u_j h}\right) + \frac{\partial}{\partial x_j}\left[U_i(\tau_{ij} - \rho\overline{u_i u_j})\right] + S_E \tag{2.14}$$

where $\rho\overline{u_j h}$ is turbulence flux term and $\frac{\partial}{\partial x_j}\left[U_i(\tau_{ij} - \rho\overline{u_i u_j})\right]$ is a viscous work term.

The mean total enthalpy is;

$$h_{tot} = h + \frac{1}{2}U_i U_i + k \tag{2.15}$$

where the turbulent kinetic energy, k is defined as:

$$k = \frac{1}{2}\overline{u^2}_i \tag{2.16}$$

Likewise, when the additional variable Φ is separated into an average component $\overline{\Phi}$ and a time-varying component $\emptyset$, the additional variable equation is written as:

$$\frac{\partial \rho \Phi}{\partial t} + \frac{\partial}{\partial x_j}(\rho U_j \Phi) = \frac{\partial}{\partial x_j}\left[\Gamma \frac{\partial \Phi}{\partial x_j} - \rho\overline{u_j \emptyset}\right] + S_\Phi \tag{2.17}$$

where $\rho\overline{u_j \emptyset}$ is the Reynolds flux.

2.3.1 Eddy Viscosity Turbulence Models

The eddy viscosity model is defined by the assumption that the turbulence consists of small eddies forming and dissipating consistently, and in which the Reynolds stresses are assumed to be proportional to mean velocity gradients. They are characterized by

the approximation including eddy viscosity and eddy diffusivity. Correspondingly, Reynolds stress term can be expressed as:

$$-\rho\overline{u_i u_j} = \mu_t\left(\frac{\partial U_i}{\partial x_j} + \frac{\partial U_j}{\partial x_i}\right) - \frac{2}{3}\delta_{ij}(\rho k + \mu_t \frac{\partial U_k}{\partial x_k}) \tag{2.18}$$

where μ_t is the eddy viscosity or turbulent viscosity.

Similar to the eddy viscosity hypothesis, according to the eddy diffusivity hypothesis, the Reynolds flux term is written as:

$$-\rho\overline{u_i \emptyset} = \Gamma_t \frac{\partial \Phi}{\partial x_i} \tag{2.19}$$

$$\Gamma_t = \frac{\mu_t}{Pr_t} \tag{2.20}$$

where Γ_t is the eddy diffusivity and Pr_t is the Prandtl number.

Based on these hypotheses, the Reynolds averaged momentum and scalar transport equations turn into:

$$\frac{\partial \rho U_i}{\partial t} + \frac{\partial}{\partial x_j}(\rho U_i U_j) = \frac{\partial p'}{\partial x_i} + \frac{\partial}{\partial x_j}\left[\mu_{eff}\left(\frac{\partial U_i}{\partial x_j} + \frac{\partial U_j}{\partial x_i}\right)\right] + S_M \tag{2.21}$$

Where S_M is the sum of the body forces and μ_{eff} effective viscosity which is defined as:

$$\mu_{eff} = \mu + \mu_t \tag{2.22}$$

and p' is a modified pressure, represented as:

$$p' = p + \frac{2}{3}\rho k + \frac{2}{3}\mu_{eff}\frac{\partial U_k}{\partial x_k} \tag{2.23}$$

The Reynolds averaged energy equation is expressed as:

$$\frac{\partial \rho h_{tot}}{\partial t} - \frac{\partial p}{\partial t} + \frac{\partial}{\partial x_j}(\rho U_j h_{tot}) = \frac{\partial}{\partial x_j}\left(\lambda \frac{\partial T}{\partial x_j} + \frac{\mu_t}{Pr_t}\frac{\partial h}{\partial x_j}\right) + \frac{\partial}{\partial x_j}\left[U_i(\tau_{ij} - \rho\overline{u_i u_j})\right] + S_E \tag{2.24}$$

and the Reynolds averaged transport equation for additional variables is described as:

$$\frac{\partial \rho \Phi}{\partial t} + \frac{\partial}{\partial x_j}(\rho U_j \Phi) = \frac{\partial}{\partial x_j}[(\Gamma_\Phi + \frac{\mu_t}{\sigma_\Phi})\frac{\partial \Phi}{\partial x_j}] + S_\Phi \tag{2.25}$$

In this part of the study, the widely used two-equation turbulence models, in which the velocity and the length scale represented by separate transport equations, are discussed.

The turbulence velocity scale is obtained from the turbulent kinetic energy and the turbulent length scale is predicted from the turbulent kinetic energy and its dissipation rate.

2.3.1.1 The κ-ε Model

The κ-ε model, which is first introduced by Launder and Spalding [88], depends on the turbulence kinetic energy (κ) represented by the variance of the fluctuations in velocity and the turbulent eddy dissipation rate (ε). Subsequently, the continuity equation is defined as:

$$\frac{\partial \rho}{\partial t} + \frac{\partial}{\partial x_j}(\rho U_j) = 0 \tag{2.26}$$

and the momentum equation is then:

$$\frac{\partial \rho U_i}{\partial t} + \frac{\partial}{\partial x_j}(\rho U_i U_j) = \frac{\partial p'}{\partial x_i} + \frac{\partial}{\partial x_j}\left[\mu_{eff}\left(\frac{\partial U_i}{\partial x_j} + \frac{\partial U_j}{\partial x_i}\right)\right] + S_M \tag{2.27}$$

where S_M demonstrates the sum of body forces and p' is the modified pressure as stated before. μ_{eff} is the effective viscosity that is expressed as:

$$\mu_{eff} = \mu + \mu_t \tag{2.28}$$

μ_t is the turbulent viscosity which can be formulated as:

$$\mu_t = C_\mu \rho \frac{k^2}{\varepsilon} \tag{2.29}$$

where C_μ is the κ-ε turbulence model constant.

The transport equations of the turbulence kinetic energy and the turbulence dissipation rate from which the κ and the ε are computed are written as:

$$\frac{\partial(\rho k)}{\partial t}+\frac{\partial}{\partial x_j}(\rho U_j k)=\frac{\partial}{\partial x_j}\left[\left(\mu+\frac{\mu_t}{\sigma_k}\right)\frac{\partial k}{\partial x_j}\right]+P_k-\rho\varepsilon+P_{kb} \tag{2.30}$$

$$\frac{\partial(\rho \varepsilon)}{\partial t}+\frac{\partial}{\partial x_j}(\rho U_j \varepsilon)=\frac{\partial}{\partial x_j}\left[\left(\mu+\frac{\mu_t}{\sigma_\varepsilon}\right)\frac{\partial \varepsilon}{\partial x_j}\right]+\frac{\varepsilon}{k}(C_{\varepsilon 1}P_k-C_{\varepsilon 2}\rho\varepsilon+C_{\varepsilon 1}P_{\varepsilon b}) \tag{2.31}$$

in which $C_{\varepsilon 1}$ and $C_{\varepsilon 2}$ are the κ-ε turbulence model constants and P_{kb} and $P_{\varepsilon b}$ symbolize the buoyancy forces and the P_k is the shear production of turbulence due to viscous forces.

2.3.1.2 The RNG κ-ε Model

Yakhot et al. [89] presented the RNG κ-ε model that is created by the renormalization group analysis of the Navier-Stokes equations. The transport equation obtained by substituting the constant $C_{\varepsilon 1\mathrm{RNG}}$ for the $C_{\varepsilon 1}$ constant in the standard κ-ε model is written as:

$$\frac{\partial(\rho \varepsilon)}{\partial t}+\frac{\partial}{\partial x_j}(\rho U_j \varepsilon)=\frac{\partial}{\partial x_j}\left[\left(\mu+\frac{\mu_t}{\sigma_\varepsilon RNG}\right)\frac{\partial \varepsilon}{\partial x_j}\right]+\frac{\varepsilon}{k}(C_{\varepsilon 1\mathrm{RNG}}P_k-C_{\varepsilon 2\mathrm{RNG}}\rho\varepsilon+C_{\varepsilon 1\mathrm{RNG}}P_{\varepsilon b}) \tag{2.32}$$

Here, the contributing terms are as follows:

$$C_{\varepsilon 1\mathrm{RNG}}=1.42-f_\eta \tag{2.33}$$

$$f_\eta=\frac{\eta(1-\frac{\eta}{4.38})}{(1+\beta_{RNG}\eta^3)} \tag{2.34}$$

$$\eta=\sqrt{\frac{P_k}{\rho C_{\mu RNG}\epsilon}} \tag{2.35}$$

2.3.1.3 The κ-ω Model

The κ-ω model introduced by Wilcox [90] that solves the transport equations for turbulent kinetic energy, κ, and turbulent frequency, ω:

$$\frac{\partial(\rho k)}{\partial t}+\frac{\partial}{\partial x_j}(\rho U_j k)=\frac{\partial}{\partial x_j}\left[\left(\mu+\frac{\mu_t}{\sigma_k}\right)\frac{\partial k}{\partial x_j}\right]+P_k-\beta'\,\rho k\omega+P_{kb} \tag{2.36}$$

$$\frac{\partial(\rho \omega)}{\partial t}+\frac{\partial}{\partial x_j}(\rho U_j \omega)=\frac{\partial}{\partial x_j}\left[\left(\mu+\frac{\mu_t}{\sigma_\omega}\right)\frac{\partial \omega}{\partial x_j}\right]+\alpha\frac{\omega}{k}P_k-\beta\,\rho\omega^2+P_{\omega b} \tag{2.37}$$

Here, P_{kb} and $P_{\omega b}$ are the buoyancy turbulence terms and the turbulence viscosity, μ_t is assumed as:

$$\mu_t = \rho \frac{k}{\omega} \tag{2.38}$$

β, β', α, σ_k, σ_ω are the model constants and the Reynolds stress tensor is expressed as:

$$-\rho\overline{u_i u_j} = \mu_t \left(\frac{\partial U_i}{\partial x_j} + \frac{\partial U_j}{\partial x_i}\right) - \frac{2}{3}\delta_{ij}(pk + \mu_t \frac{\partial U_k}{\partial x_k}) \tag{2.39}$$

2.3.1.4 The Shear Stress Transport (SST) Model

The shear stress transport model developed by Menter [91] aimed to obtain transport behavior by imposing restriction to the calculation of the eddy viscosity:

$$v_t = \frac{\alpha_1 k}{\max(\alpha_1 \omega, SF_2)} \tag{2.40}$$

$$v_t = \mu_t / \rho \tag{2.41}$$

Where S is an invariant measure of the strain rate and F_2 is the blending function that is defined as:

$$F_2 = \tanh(arg_2^2) \tag{2.42}$$

with:

$$arg_2 = \max\left(\frac{2\sqrt{k}}{\beta'\omega y}, \frac{500\, v}{y^2 \omega}\right) \tag{2.43}$$

where y is the distance to the nearest wall and v is the kinematic viscosity.

2.3.2 Reynolds Stress Turbulence Models

The Reynolds stress models, depending on all components of the Reynolds stress tensor and the dissipation rate, deals with the transport equation by solving the individual stress components. Thus, the Reynolds averaged momentum equation for the mean velocity is written as:

$$\frac{\partial \rho U_i}{\partial t} + \frac{\partial}{\partial x_j}\left(\rho U_i U_j\right) - \frac{\partial}{\partial x_j}\left[\mu\left(\frac{\partial U_i}{\partial x_j} + \frac{\partial U_j}{\partial x_i}\right)\right] = -\frac{\partial p''}{\partial x_i} - \frac{\partial}{\partial x_j}(\rho\overline{u_\iota u_\jmath}) + S_{M_i} \tag{2.44}$$

Here, S_{M_i} is the sum of the body forces, p'' is a modified pressure that is expressed as:

$$p'' = p + \frac{2}{3}\mu\frac{\partial U_k}{\partial x_k} \tag{2.45}$$

The fluctuating Reynolds stress component $\rho\overline{u_\iota u_\jmath}$ satisfies the differential Reynolds stress transport equation which is defined as:

$$\frac{\partial \rho\overline{u_\iota u_\jmath}}{\partial t} + \frac{\partial}{\partial x_k}\left(U_k\rho\overline{u_\iota u_\jmath}\right) - \frac{\partial}{\partial x_k}\left[\left(\delta_{kl}\mu + \rho C_S\frac{k}{\varepsilon}\overline{u_k u_l}\right)\frac{\partial\overline{u_\iota u_\jmath}}{\partial x_l}\right] = P_{ij} - \frac{2}{3}\delta_{ij}\rho\varepsilon + \Phi_{ij} + P_{ij},b \tag{2.46}$$

Where P_{ij} and P_{ij},b are shear and buoyancy turbulence production terms of the Reynolds stresses respectively, Φ_{ij} is the pressure strain tensor and C is a constant.

2.3.2.1 ω-Based Reynolds Stress Model

The ω-Reynolds stress model is found out based on the ω equation. In this study, the ω-Reynolds stress model is used among the Reynolds stress models. Therefore, the equation for Reynolds stresses is written as:

$$\frac{\partial \rho\overline{u_\iota u_\jmath}}{\partial t} + \frac{\partial}{\partial x_k}\left(U_k\rho\overline{u_\iota u_\jmath}\right) = P_{ij} - \frac{2}{3}\beta'\rho\omega k\delta_{ij} + \Phi_{ij} + P_{ij,b} + \frac{\partial}{\partial x_k}\left[\left(\mu + \frac{\mu_t}{\sigma_k}\right)\frac{\partial\overline{u_\iota u_\jmath}}{\partial x_k}\right] \tag{2.47}$$

And the equation for ω reads:

$$\frac{\partial(\rho\omega)}{\partial t} + \frac{\partial(U_k\rho\omega)}{\partial x_j} = \alpha\rho\frac{\omega}{k}P_k + P_{\omega b} - \beta\,\rho\omega^2 + \frac{\partial}{\partial x_k}\left[\left(\mu + \frac{\mu_t}{\sigma}\right)\frac{\partial\omega}{\partial x_k}\right] \tag{2.48}$$

Where σ, α, β and $\beta'$are constants.

2.3.3 The κ-ε Explicit Algebraic Reynolds Stress (EARSM) Model

Explicit Algebraic Reynolds Stress models were created by developing the standard two-equation models. In this model, the Reynolds stresses are given by:

$$\overline{u_\iota u_\jmath} = k(\alpha_{ij} + 2/3\delta_{ij}) \tag{2.49}$$

Here the anisotropy tensor α_{ij}, strain rate tensor S_{ij} and vorticity tensor Ω_{ij} are defined as:

$$\alpha_{ij} = \beta_1 S_{ij} + \beta_3 \left(\Omega_{ik}\Omega_{kj} - \frac{1}{3} II_\Omega \delta_{ij}\right) + \beta_4 \left(S_{ik}\Omega_{kj} - \Omega_{ik}S_{kj}\right) + \beta_6 \left(S_{ik}\Omega_{kl}\Omega_{lj} + \Omega_{ik}\Omega_{kl}S_{lj} - \frac{2}{3} IV \delta_{ij}\right) + \beta_9 \left(\Omega_{ik}S_{kl}\Omega_{lm}\Omega_{mj} - \Omega_{ik}\Omega_{kl}S_{lm}\Omega_{mj}\right) \quad (2.50)$$

$$S_{ij} = \frac{1}{2}\tau\left(\frac{\partial U_i}{\partial x_j} + \frac{\partial U_j}{\partial x_i}\right) \quad (2.51)$$

$$\Omega_{ik} = \frac{1}{2}\tau\left(\frac{\partial U_i}{\partial x_j} + \frac{\partial U_j}{\partial x_i}\right) \quad (2.52)$$

where τ denotes the time scale reads:

$$\tau = \max\left(\frac{1}{\beta^* \omega}; C_\tau \sqrt{\frac{v}{\beta^* k \omega}}\right) \quad (2.53)$$

C_τ and β^* are constants and the coefficients mentioned are as follows:

$$\beta_1 = -N(2N^2 - 7II_\Omega)/Q \quad (2.54)$$

$$\beta_3 = -12IV/NQ \quad (2.55)$$

$$\beta_4 = -2(N^2 - 2II_\Omega)/Q \quad (2.56)$$

$$\beta_6 = -6N/Q \quad (2.57)$$

$$\beta_9 = 6/Q \quad (2.58)$$

$$Q = \frac{5}{6}(N^2 - 2II_\Omega)(2N^2 - II_\Omega) \quad (2.59)$$

$$II_S = S_{kl}S_{lk} \quad (2.60)$$

$$II_\Omega = \Omega_{kl}\Omega_{lk} \quad (2.61)$$

$$IV = S_{kl}\Omega_{lm}\Omega_{mk} \quad (2.62)$$

The N function is expressed as:

$$N = \begin{cases} \frac{A_3}{3} + (P_1 + \sqrt{P_2})^{1/3} + sign\left(P_1 - \sqrt{P_2}\right)\left|P_1 - \sqrt{P_2}\right|^{\frac{1}{3}}, & P_2 \geq 0 \\ \frac{A_3'}{3} + 2(P_1^2 + P_2)^{1/6} + cos\left(\frac{1}{3} arccos\left(\frac{P_1}{\sqrt{P_1^2 - P_2}}\right)\right), & P_2 < 0 \end{cases} \tag{2.63}$$

$$P_1 = \left(\frac{A_3'^2}{3} + \frac{9}{20} II_S - \frac{2}{3} II_\Omega\right) A_3' \tag{2.64}$$

$$P_2 = P_1^2 - \left(\frac{A_3'^2}{3} + \frac{9}{10} II_S - \frac{2}{3} II_\Omega\right)^3 \tag{2.65}$$

$$A_3' = \frac{9}{5} + \frac{9}{4} C_{diff} \max(1 + \beta_1^{(eq)} II_S; 0) \tag{2.66}$$

$$\beta_1^{(eq)} = -\frac{6}{5} \frac{N^{(eq)}}{(N^{(eq)})^2 - 2II_\Omega} \tag{2.67}$$

where $N^{(eq)}$ and C_{diff} are constants. The eddy viscosity is defined as:

$$v_t = C_\mu k\tau \tag{2.68}$$

where

$$C_\mu = -\frac{1}{2}(\beta_1 + II_\Omega \beta_6) \tag{2.69}$$

3. COMPUTATIONAL FLUID DYNAMICS SIMULATION

CFD is a computer-based tool used to analyze numerically the physical phenomena such as fluid flow and heat transfer in which the equations of the fluid motion are solved over the studied region considering the boundary and initial conditions. In this study, Ansys Workbench and Ansys CFX, as a CFD tool, are used to evaluate the performances of the turbulence models in terms of predicting the pressure gradients of the systems of interest. The accuracy of the CFD results is verified with the experimental data.

3.1 Computational Method

Ansys CFX is a high-performance computational fluid dynamics (CFD) software tool that provides reliable and fast solutions in a wide range of engineering applications including pre-processing, solver, and post-processing stages. The procedure to be followed to perform a CFD analysis is shown in Figure 3.1

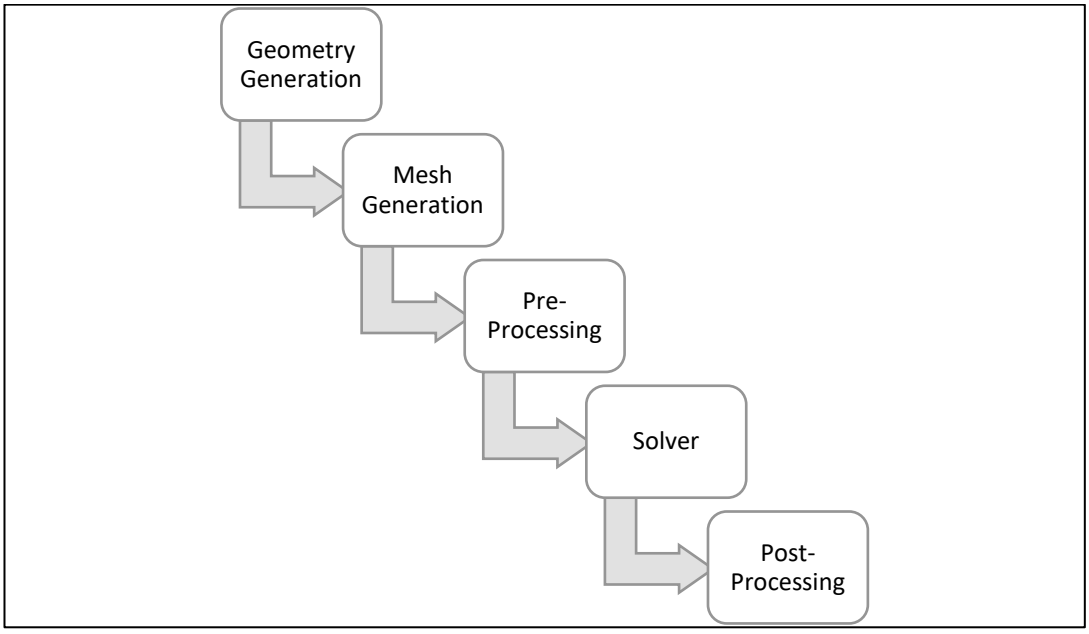

Figure 3.1 Flow Chart of the ANSYS CFX.

In the pre-processing stage, the 3-D model is developed for the water flow in rough pipe, concentric and eccentric annulus, and sediment transport in the concentric annulus. Two geometries are generated for rough pipe with diameters of 80 and 90 mm. The geometry generation process of the rough pipe is shown as an example in Figure 3.2 The eccentric and concentric annulus geometries for the water flow are created to have 40-80 mm and 46-74 mm diameters, respectively. The geometry of the eccentric annulus for sediment transport is created to be 46-92 mm diameters.

The geometry and the computational mesh have been generated in the geometry and mesh applications of the CFD program (ANSYS R15), representatively the geometry and the mesh structure of annulus is shown in Figure 3.3, Figure 3.4

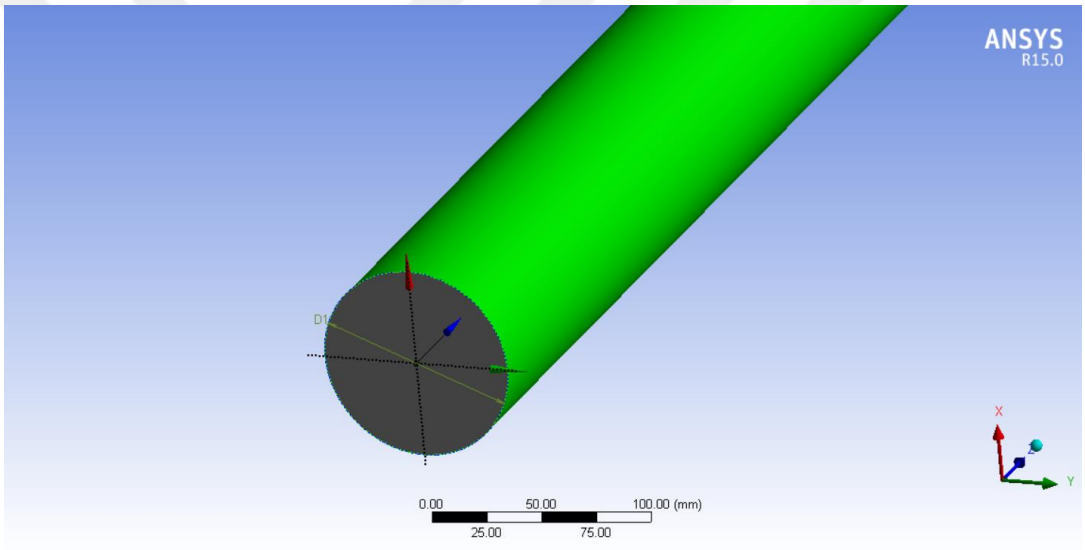

Figure 3.2 Rough pipe geometry generation in ANSYS.

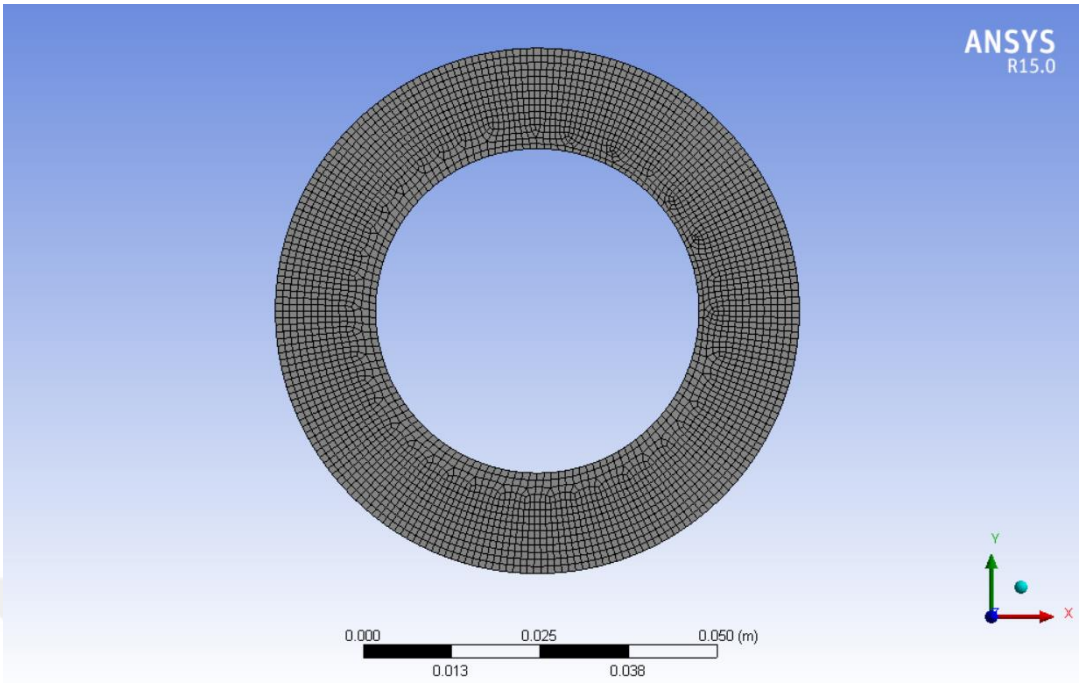

Figure 3.3 Concentric annulus computational mesh.

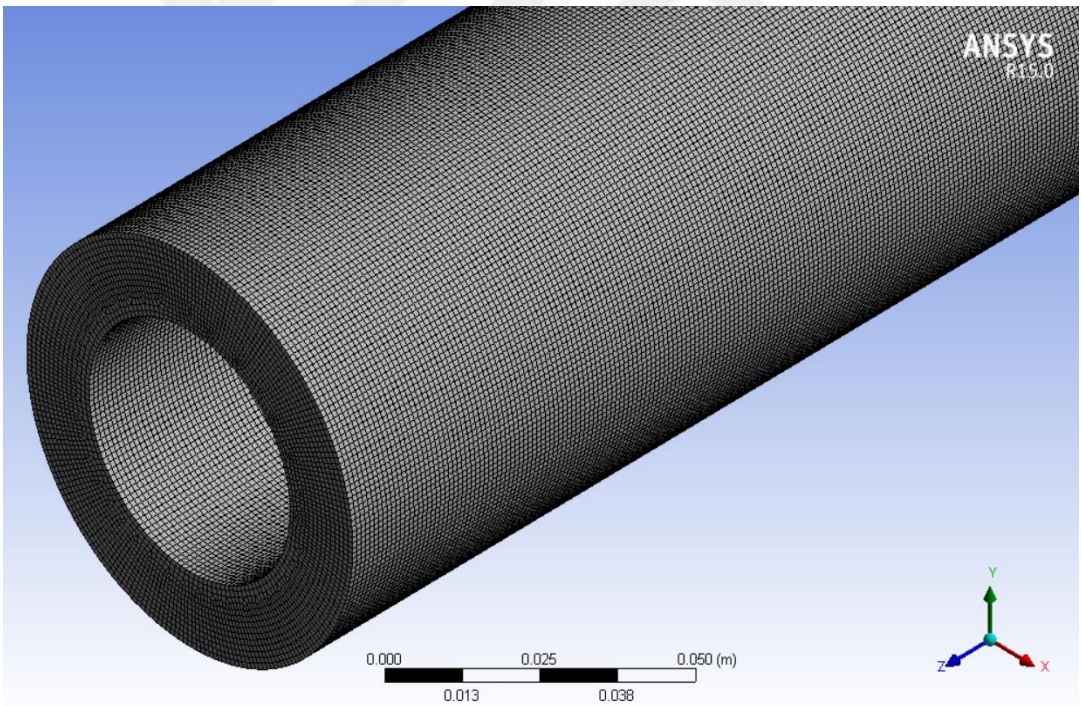

Figure 3.4 Concentric annulus geometry.

The mesh independence analysis has been performed and the optimum mesh sizes for all cases are implemented. As an example of the determination of optimum mesh for the concentric annulus is presented in Figure 3.5.

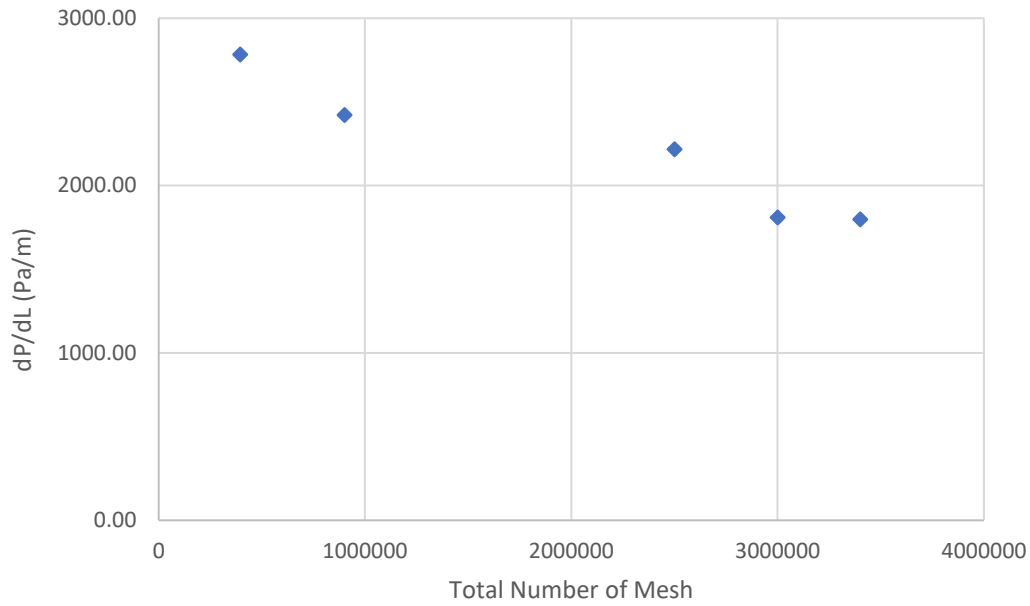

Figure 3.5 Determination of optimum mesh for the concentric annulus.

In the solver part of the CFD program, the required initial and boundary conditions are described. The uniform velocity at the domain inlet and the atmospheric pressure at the domain outlet are applied. Figure 3.6 and Figure 3.7 exemplify the implementation of the inlet and the outlet boundary conditions. The flow is assumed to be steady, incompressible, isothermal, and statistical turbulence models are employed to simulate the pipeline system. In addition, for the annular flow, the no-slip condition is applied at the inner wall and the thermal conditions presented in Table 3.1.

For the rough pipe, relative roughnesses are applied as 0.001 and 0.0013. For the sediment transport, the water and the sediment are defined as separate materials. The sediment particle is introduced to the system with a diameter of 2 mm and a density of 1800 kg/m^3.

Table 3.1 Thermal Conditions of Water.

	25°C	40°C	50°C	60°C
Density (kg/m^3)	997	998	998	998
Specific Heat Capacity ($Jkg^{-1}K^{-1}$)	4181.7	4179	4181	4185
Thermal Conductivity ($Wm^{-1}K^{-1}$)	0.6069	0.631	0.644	0.654
Thermal Expansivity (K^{-1})	0.000257	0.000458	0.000458	0.000458
Dynamic Viscosity ($kgm^{-1}s^{-1}$)	0.000890	0.000653	0.000547	0.000467

The most important and final stage of the solver part continues with the calculations and iterations. Figure 3.8 represents an example image of the running process.

In the post-processing stage, the results are visualized and analyzed. The pressure distribution in the eccentric annulus is illustrated in Figure 3.9 as an example.

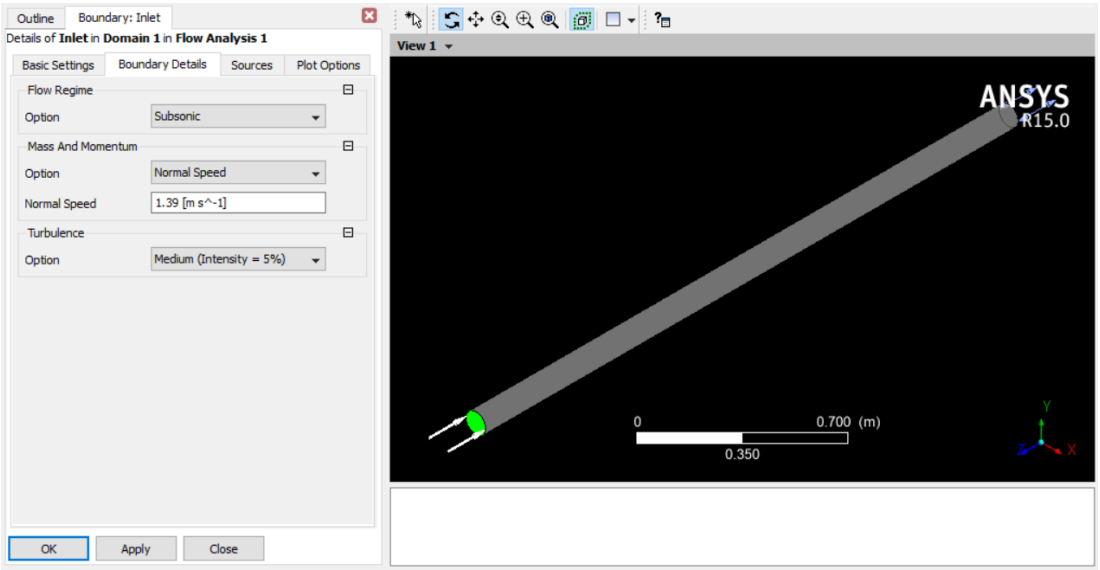

Figure 3.6 Implementation of the inlet boundary condition.

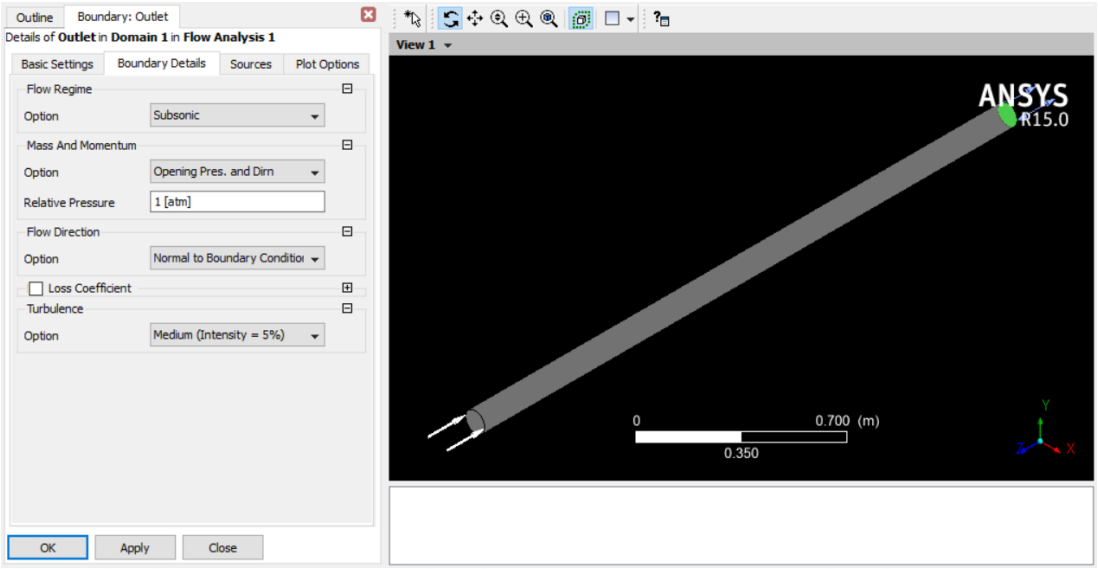

Figure 3.7 Implementation of the outlet boundary condition.

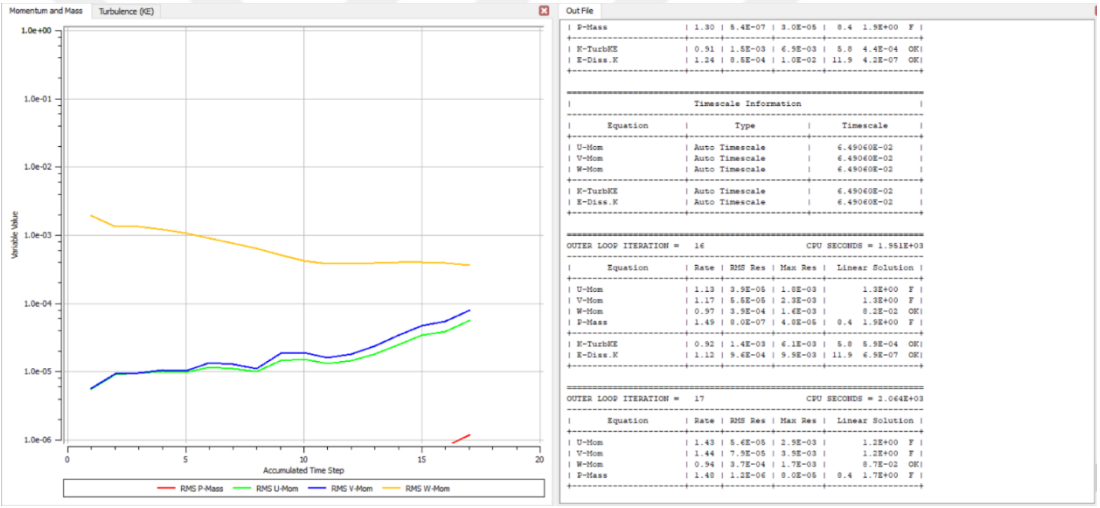

Figure 3.8 Running process of the problem.

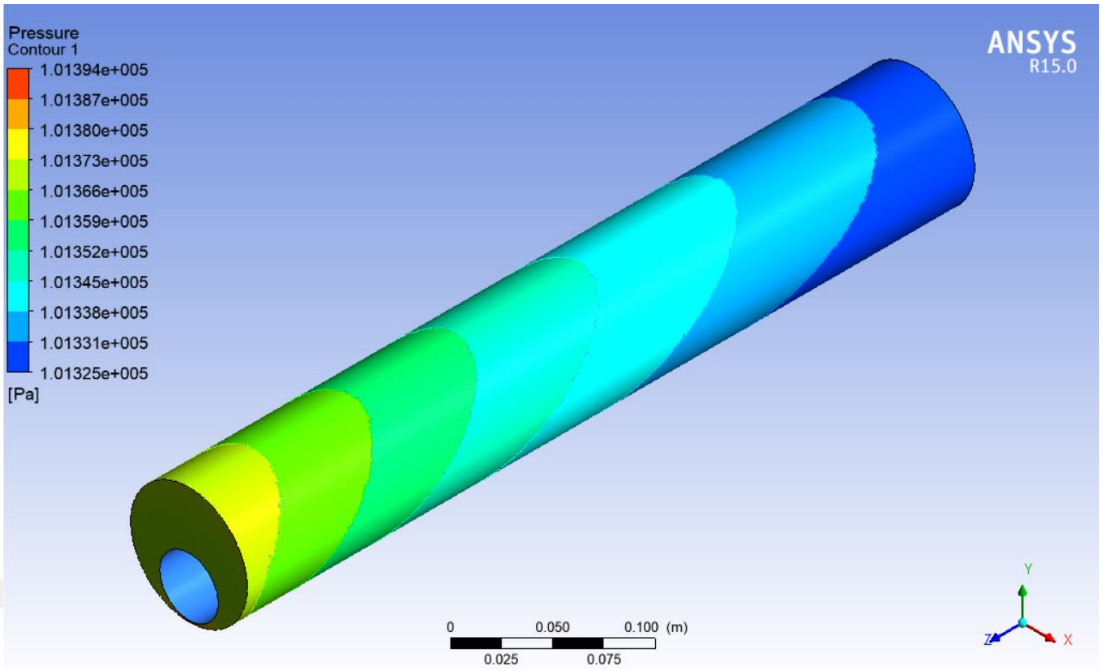

Figure 3.9 Pressure distribution in eccentric annulus.

4. EXPERIMENTAL SETUP

In this study, the results obtained from the CFD simulations are verified with the experimental data obtained from separate studies. The experiments were conducted for both sediment transport and single-phase flow.

The experiments for flow through the 80 and 90 mm-diameter rough pipes were conducted in İzmir Katip Celebi University, Civil Engineering Flow Loop (Figure 4.1). The experimental facility consisted of a pump, pressure transducer, control valves, water tank, flow meter, and the rough pipe.

Figure 4.1 Izmir Katip Celebi University Civil Engineering Department Flow Loop, rough pipe.

The test section of the rough pipe system was 10 m and the relative roughness values were 0.001 and 0.0013 for 80 mm-diameter and 90 mm-diameter pipes respectively. During the experiments, flow rate ranges were between 16 m3/h-90 m3/h. The experiment specifications are given in Table 4.1.

Table 4.1 Test parameter values during the experiments, rough pipe.

Experiment Specifications	Values
Pipe diameter	80,90 mm
Flow loop length	10 m
Flow rate range	16-90 m^3/h
Relative roughness	0.001, 0.0013

Experiments for water flow in eccentric annulus were also conducted in İzmir Katip Celebi University, Civil Engineering Flow Loop (Figure 4.2).

Figure 4.2 Izmir Katip Celebi University Civil Engineering Department Flow Loop, eccentric annulus.

The length of the experimental test section was 10 m and it consisted of 80 mm outer and 40 mm inner diameters. Experiments were performed for a flow rate range of 6.9 m^3/h-31.4 m^3/h and a temperature range of 25°C – 60°C degrees are given in Table 4.2.

Table 4.2 Test parameter values during the experiments, water flow in eccentric annulus [2].

Experiment Specifications	Values
Inner- outer pipe diameter	40-80 mm
Flow loop length	10 m
Flow rate range	6.9-31.4 m^3/h
Temperature	25,40,50 and 60°C

The experimental setup consisted of a pump, pressure transducer, control valves, water tank, flow meter, and the annular test section. Differential pressure loss data in fully developed flow regions were read from digital pressure transmitters recorded by the data logger.

Experimental studies for the water flow in the concentric annulus and sediment transport in eccentric annulus were conducted by Sorgun [1] in Middle East Technical University, Petroleum Engineering Flow Loop (Figure 4.3). The experimental setup consisted of sediment collection and injection tanks, liquid tank, shale shaker, pumps, control valve, compressor, annular test section, pipe rotation system, pressure transducer, and data acquisition system.

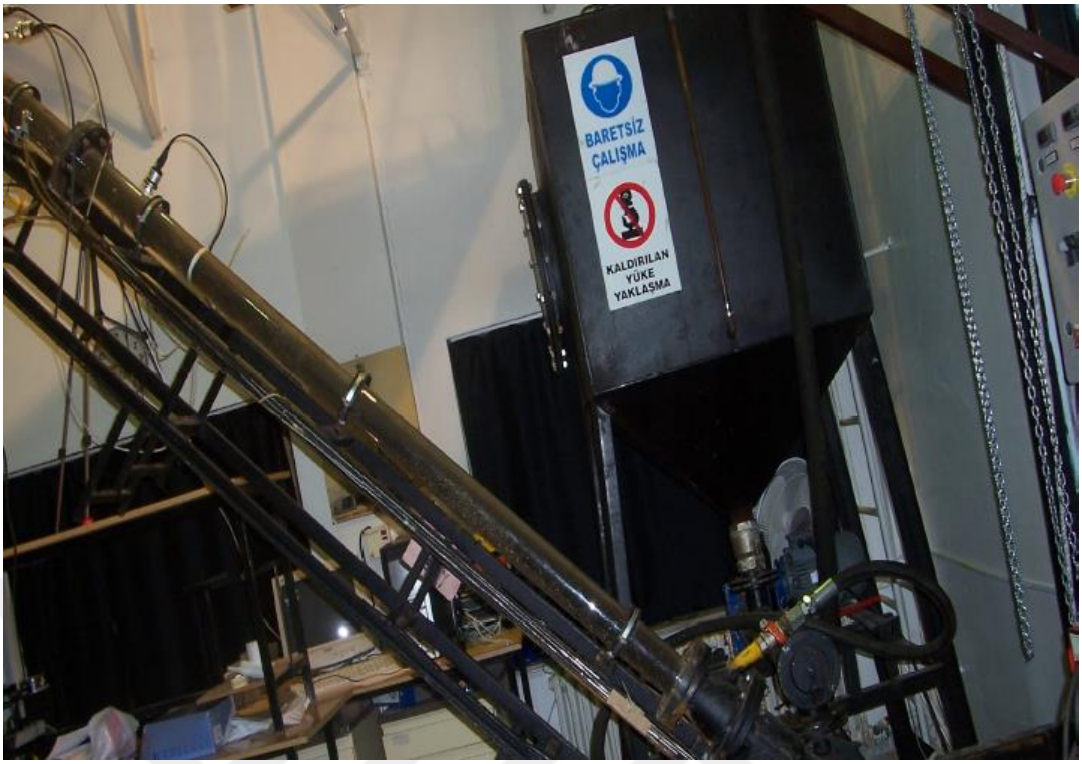

Figure 4.3 Middle East Technical University Petroleum Engineering Department Flow Loop, annular test section.

The 3.65 m long horizontal pipeline consisted of a 46 mm inner and 74 mm outer diameters for concentric annulus and the experiments were performed for a flow rate range of 6.1 m^3/h-21.6 m^3/h.

The experiments of the sediment transport were conducted in the 46 mm inner and 74 mm outer diameters eccentric annulus with a length of 3.65 m. The flow rate ranges were recorded between 6.1-15.9 m^3/h. Experiment specifications are given in Table 4.3. and Table 4.4.

Table 4.3 Test parameter values during the experiments, water flow in the concentric annulus.

Experiment Specifications	Values
Inner- outer pipe diameter	46-74 mm
Flow loop length	3.65 m
Flow rate range	6.1-21.6 m^3/h

Table 4.4 Test parameter values during the experiments, the eccentric annulus, sediment transport.

Experiment Specifications	Values
Inner- outer pipe diameter	46-74 mm
Flow loop length	3.65 m
Flow rate range	6.1-15.9 m^3/h
Rate of penetration range	0.0013-0.0101 m/s

5. RESULTS AND DISCUSSION

In this study, the numerical simulations have been carried out for the flow through rough pipe and annulus under various conditions with several turbulence models by using CFD software ANSYS CFX. Experimental data are used to verify the reliability of the CFD simulations. The performances of the turbulence models are thoroughly discussed in terms of the pressure gradient to understand which turbulence model gives the appropriate results. The evaluation of the results based on the error metrics is also presented by utilizing the Average Absolute Percentage Error (AAPE). This is important to correctly interpret the results.

AAPE is defined as:

$$AAPE = \frac{1}{n}\sum_{t=1}^{n}\left|\frac{A_t - F_t}{A_t}\right| \tag{2.70}$$

Here, n denotes the number of the sample which is available in the data set, A_t represents the predicted value and F_t represents the measured value.

5.1 Water Flow Through The Rough Pipe

The work on the water flow through rough pipe have been carried out for two different flow loops with diameters of 80 and 90 mm. The pressure gradients have been obtained for the flow rates from 16 to 90 m^3/h. The comparison of the calculated pressure gradient values versus measured ones during the experiments for 80 and 90-mm diameter rough pipes are given in Figure 5.1 and Figure 5.2, respectively.

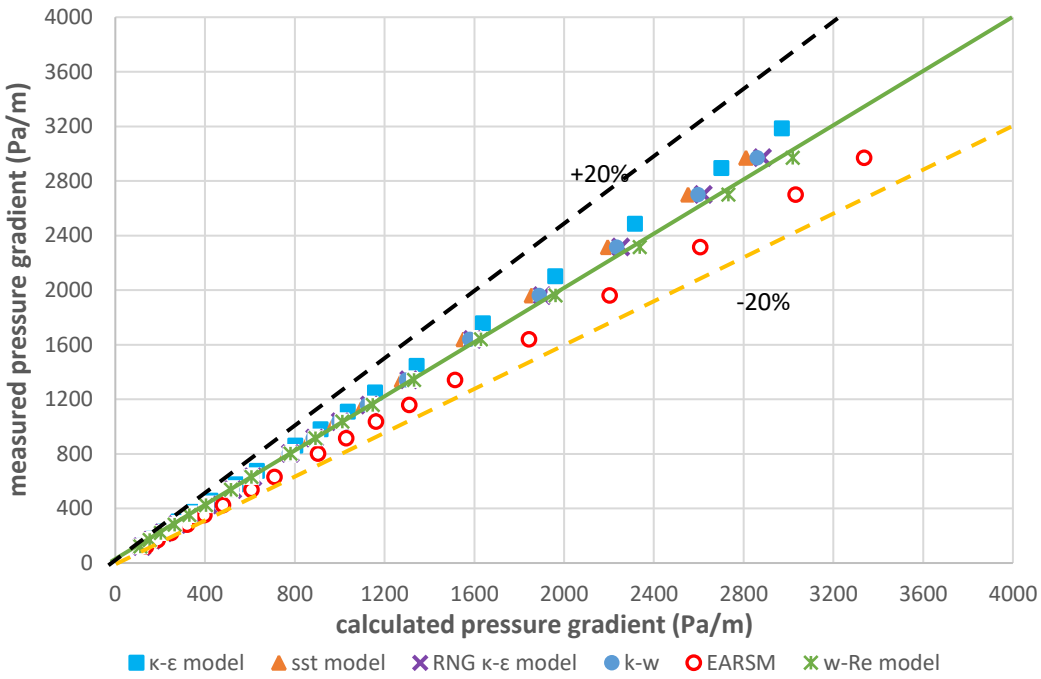

Figure 5.1 Measured versus calculated pressure gradient (Pa/m), 80 mm rough pipe.

In Figure 5.1, the calculated and measured pressure gradients are given in the x-axis and y-axis respectively, the perfect line illustrated as a solid line, and the dashed lines represent the ± 20% percent error ranges. As can be seen from the graph, the results remain within the specified error limit and the ω –Re stress and RNG κ-ε models give the best results which are very close to each other.

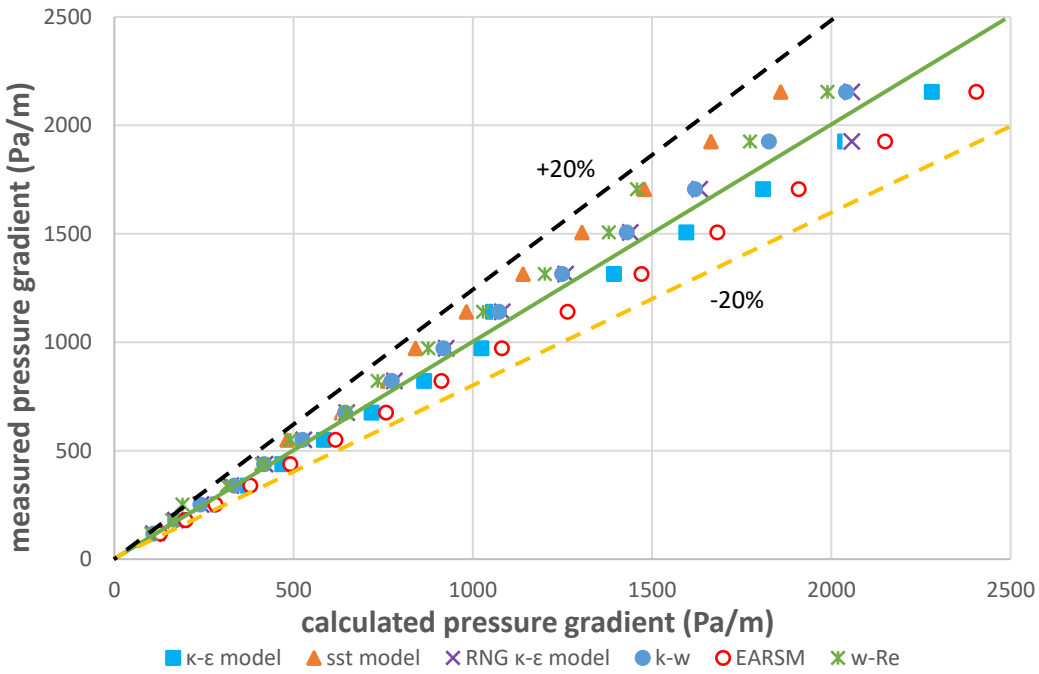

Figure 5.2 Measured versus calculated pressure gradient (Pa/m), 90 mm pipe diameter.

Figure 5.2 shows that the simulation results give good agreement with the experimental data. It can be seen from the graph, the RNG κ-ε and κ- ω models outperform the other models.

In Table 5.1., AAPE stands for average absolute percent error and demonstrates the consistency between the results of the different turbulence models obtained from CFD analysis and those from the experiments. According to the Table 5.1., it can also be said that the RNG κ-ε and κ- ω models perform better than the other turbulence models for the 80-mm diameter rough pipe, in terms of the error analysis.

Table 5.1 Performance comparison of turbulence models based on AAPE, 80 mm pipe diameter.

AAPE					
κ-ε	SST	RNG κ-ε	κ-ω	ω -Re	EARSM
7.37	5.04	2.72	3.42	2.59	12.68

Table 5.2 Performance comparison of turbulence models based on AAPE, 90 mm pipe diameter.

AAPE					
κ-ε	SST	RNG κ-ε	κ-ω	ω -Re	EARSM
5.72	9.98	4.69	4.94	10.07	11.53

It can be understood from Table 5.2., that the results of κ-ω and RNG κ-ε models are in coordination with the experimental results for 90 mm-diameter rough pipe when considering the error metric.

Overall, the results confirm that the RNG κ-ε model is a good choice for the analysis of rough pipes. It is also seen that the error margins increase as the diameter increases.

5.2 The Annular Flow

In this part, the results of the CFD simulations performed for the water flow in both the eccentric annulus and the concentric annulus are comparatively reviewed.

5.2.1 Water Flow Through The Eccentric Annulus Including Temperature Effect

The pressure gradient values are described for the water flow in the eccentric annulus. At the same time, the temperature effect is investigated by both experimenting and modeling for the specified temperature values. Figure 5.3 - Figure 5.6 indicate that the comparisons of the pressure gradients predicted by CFD with the measured ones for the water flow in the eccentric annulus at the temperatures of 25°C, 40°C, 50°C, and 60°C, respectively.

It can be seen from Figure 5.3, the results obtained from the CFD analysis are broadly in line with those from the experimental work. It is observed that the RNG k-ε and the κ-ε models give outstanding results for the water flow in the eccentric annulus at 25 °C.

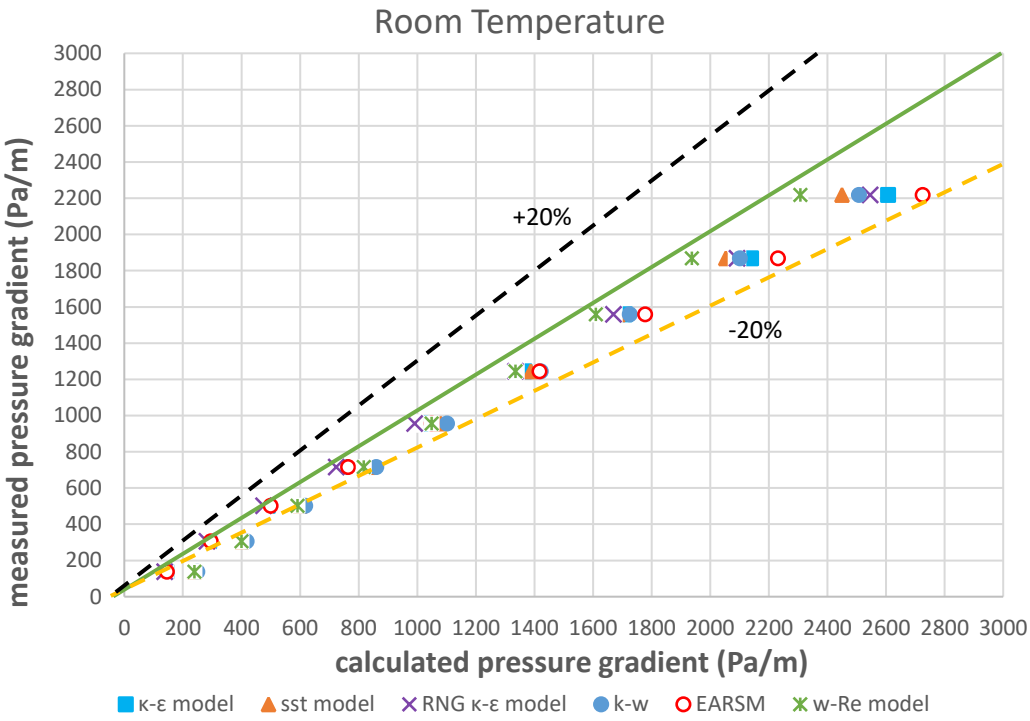

Figure 5.3 Measured versus calculated pressure gradient (Pa/m), eccentric annulus, T=25°C.

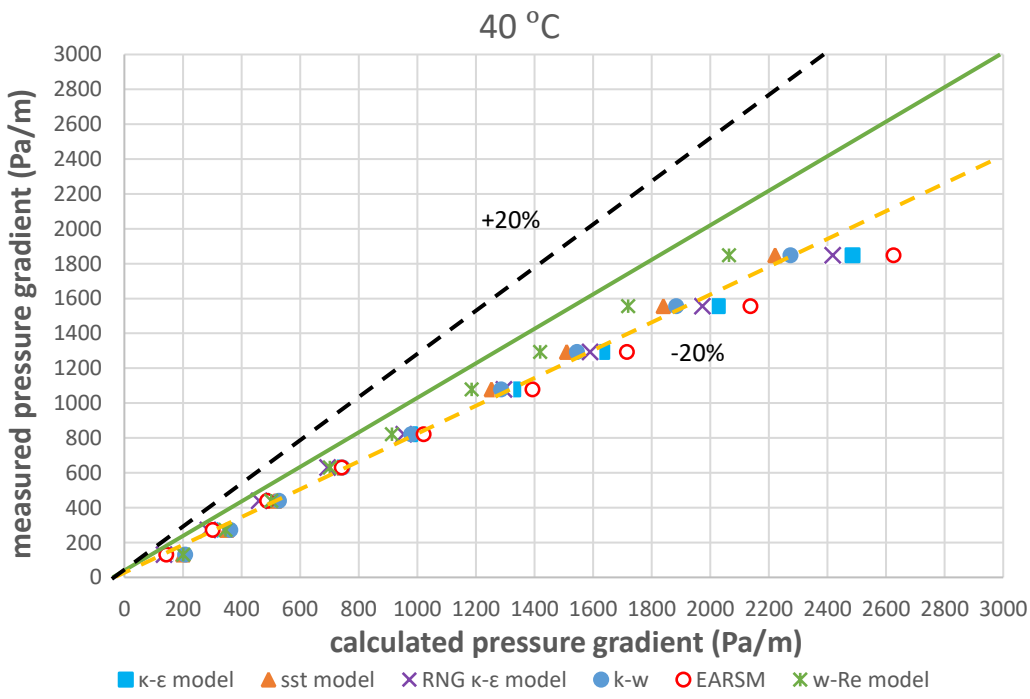

Figure 5.4 Measured versus calculated pressure gradient (Pa/m), eccentric annulus, T=40°C.

Figure 5.4 shows that the turbulence model results are at acceptable intervals when comparing the experimental ones and the RNG k-ε model performs better than the other turbulence models in the analysis of the water flow in the eccentric annulus at 40°C.

As can be seen in Figure 5.5, the ω -Re model performs quite well at the 50°C water flow in the eccentric annulus, while the performances of other turbulence models can be interpreted as having close results.

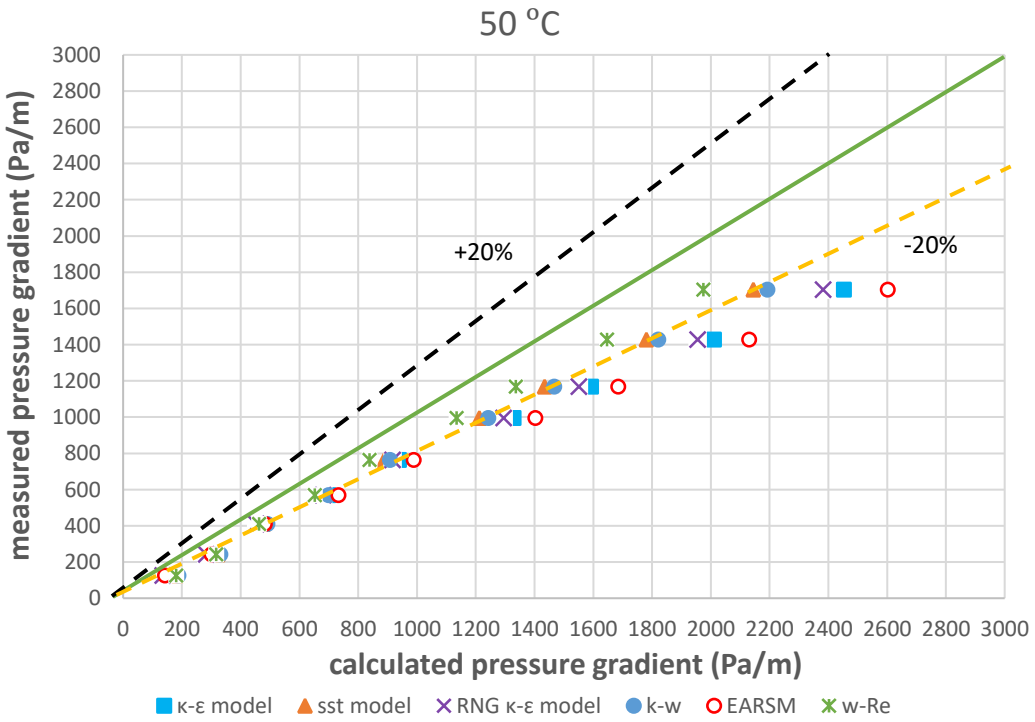

Figure 5.5 Measured versus calculated pressure gradient (Pa/m), eccentric annulus, T=50°C.

When Figure 5.6 is considered, the ω-Re model shows rather good behavior, meanwhile, the other models also give similar results for the 60°C water flow in the eccentric annulus.

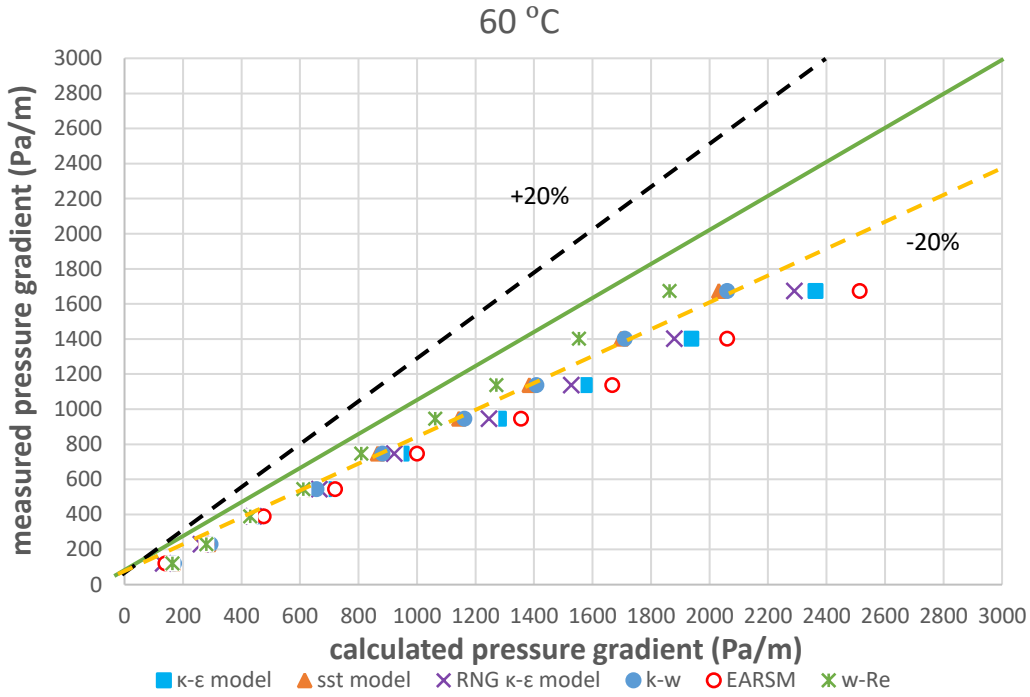

Figure 5.6 Measured versus calculated pressure gradient (Pa/m), eccentric annulus, T=60°C.

When the data collected from the analysis of the water flow in the eccentric annulus are examined according to the error metric as stated in Table 5.3., the RNG κ-ε model provides more accurate results than the other turbulence models at the lower temperatures. Together, the present findings confirm that the accuracy of the RNG κ-ε model decreases with the increasing temperature.

In general, the CFD analysis on the water flow in the eccentric annulus implies that the turbulence models give satisfactory results. The RNG κ-ε model predicts the pressure loss from room temperature to high temperatures accurately enough, nevertheless, it should be noted that the ω -Re model performs better at 50°C and 60°C.

Table 5.3 Performance comparison of turbulence models based on AAPE, eccentric annulus.

	AAPE					
Temperature(°C)	κ-ε	SST	RNG κ-ε	κ-ω	ω -Re	EARSM
25	8.16	21.71	6.59	25.32	18.46	10.73
40	19.06	22.80	15.96	26.29	18.23	24.30
50	26.88	24.76	23.54	28.12	18.88	33.23
60	27.99	21.96	24.41	24.02	15.03	34.83

5.2.2 Water Flow Through The Concentric Annulus

The water flow in the concentric annulus is analyzed by considering the pressure gradient values. Figure 5.7 shows that superior results are seen for the EARSM model when compared to the other turbulence models.

When the results are criticized in terms of error margins, as it is seen in Table 5.4., in contrast to other models, κ-ε and EARSM models have high performance in estimating the pressure gradient values and achieve approximate results. It can also be clearly said that the other turbulence models give inadequate results.

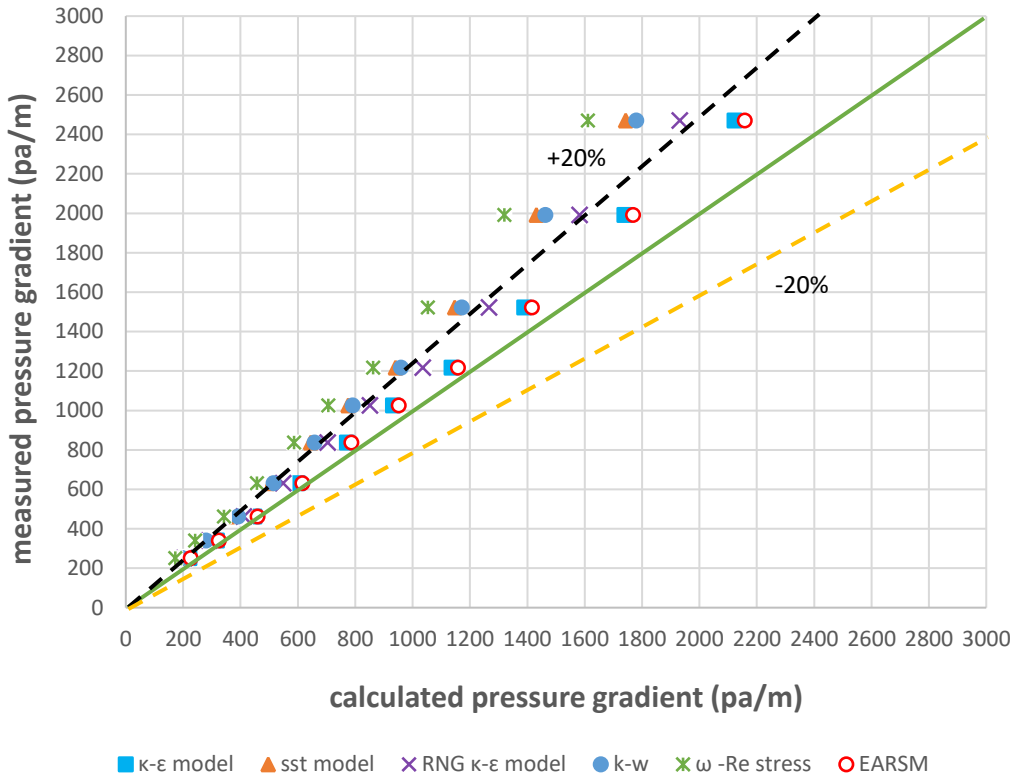

Figure 5.7 Measured versus calculated pressure gradient (Pa/m), concentric annulus.

Table 5.4 Performance comparison of turbulence models based on AAPE, concentric annulus.

AAPE					
κ-ε	SST	RNG κ-ε	κ-ω	ω -Re	EARSM
7.82	22.44	15.71	20.77	29.69	5.86

5.2.3 Sediment Transport In The Eccentric Annulus

When the sediment transport in eccentric annulus analyzed, all turbulence models give close results. It can be found out that from Figure 5.8 that the κ-ω model is in good agreement with the measured data. It is also come out that ω based turbulence models provide better results when compared with the other turbulence models.

If the analysis of the sediment transport in the eccentric annulus evaluated according to the error metric, as shown in Table 5.5., the κ-ω and ω –Re Stress models give the best results. These results also reveal that the other turbulence models also give approximate results. Sediment transport in the eccentric annulus is modeled by using the CFD program, the simulation example is shown in Figure 5.9

Velocity contour plots for the sediment transport in the eccentric annulus are presented in Figures 5.10-5.11 In Figure 5.10, sediment accumulation is observed at the wider part of the pipe. When the minimum and maximum velocity profiles are analyzed, it can be understood that the sediment transport in the wider part significantly increases while fluid velocity increases.

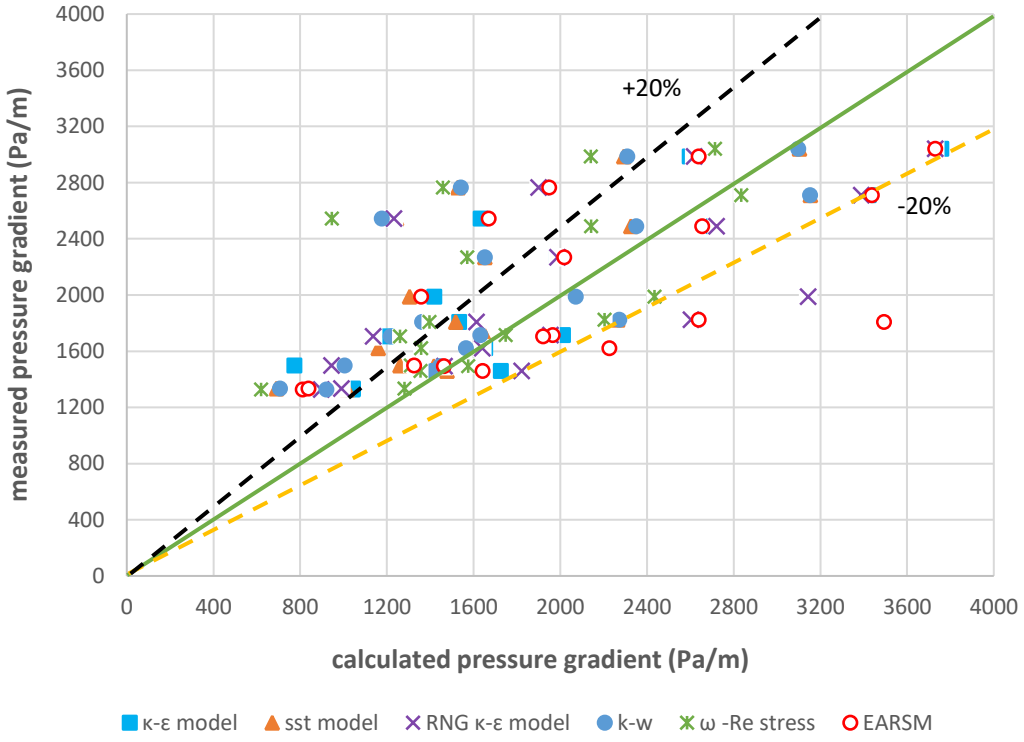

Figure 5.8 Measured versus calculated pressure gradient (Pa/m), sediment transport.

Table 5.5 Performance comparison of turbulence models based on AAPE, sediment transport.

AAPE					
κ-ε	SST	RNG κ-ε	κ-ω	ω -Re	EARSM
22.16	22.54	24.79	21.09	21.74	26.60

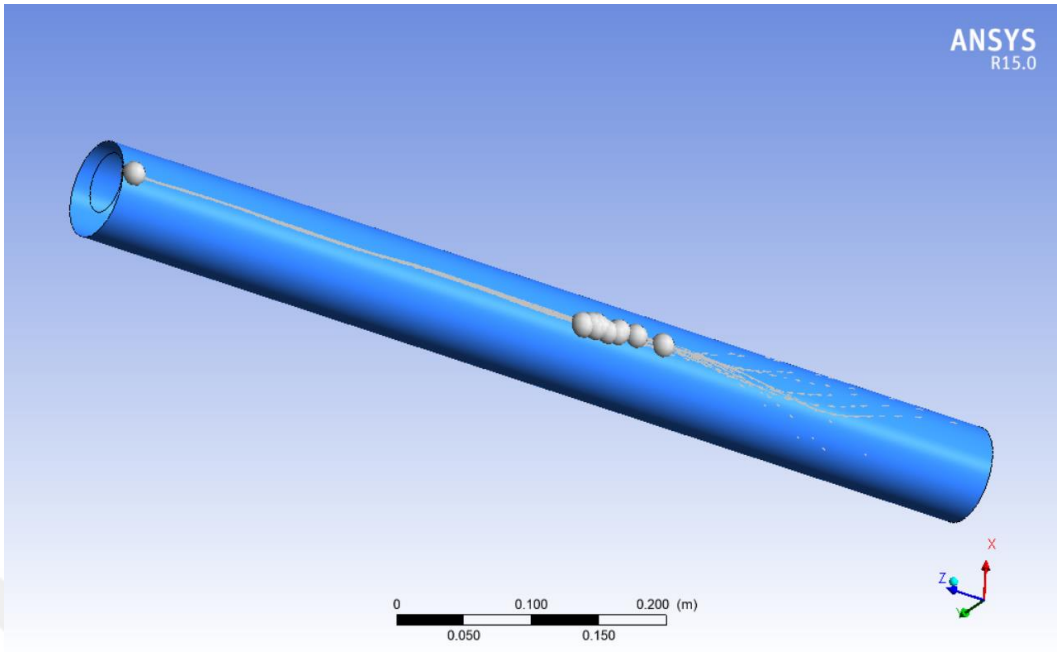

Figure 5.9 Simulation of the sediment transport in the eccentric annulus.

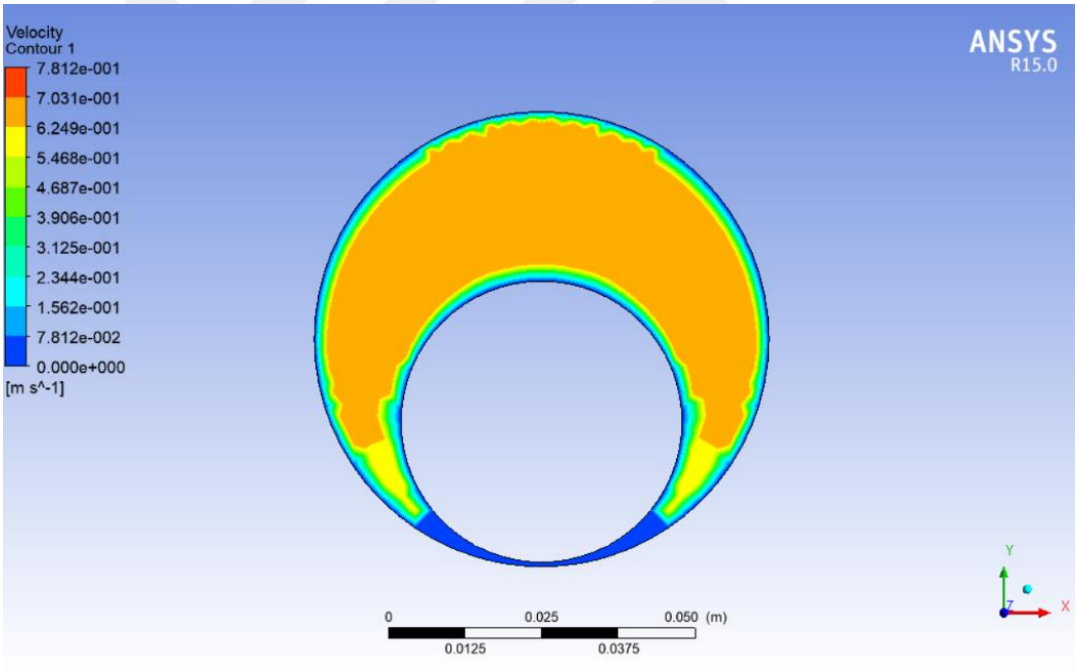

Figure 5.10 Velocity contour plot of sediment transport, v=2.1 m/s.

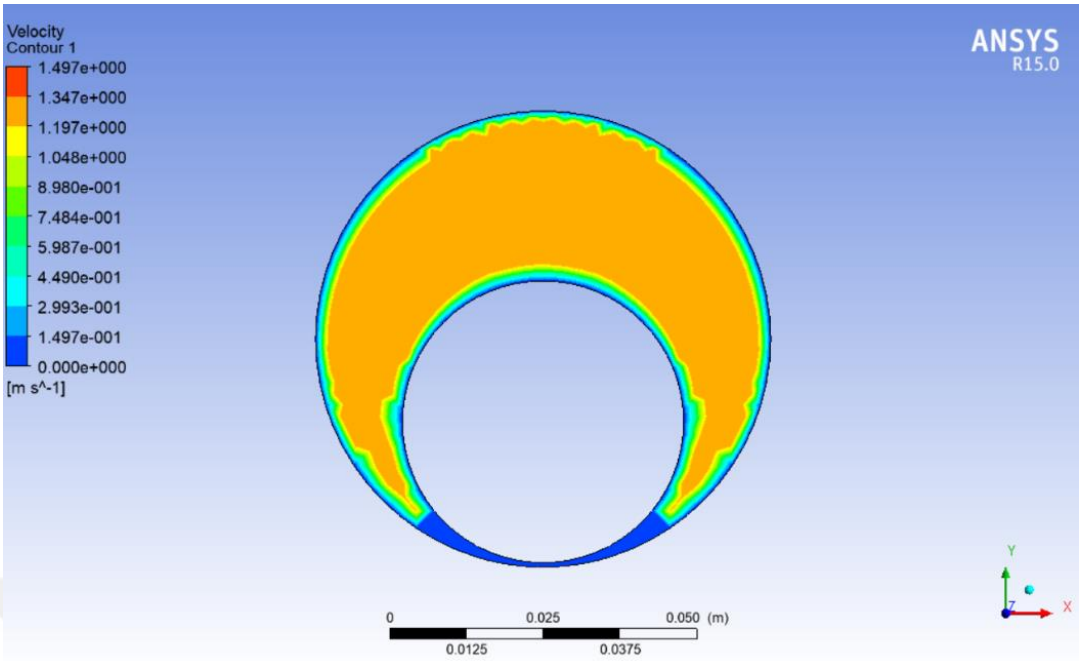

Figure 5.11 Velocity contour plot of sediment transport, v=4.2 m/s.

6. CONCLUSIONS

This study presents important findings in the understanding of the working mechanism of the turbulence models under various flow conditions. CFD simulations have been carried out for various pipeline systems to determine the performance of the statistical turbulence models by using commercial software program ANSYS R15. The pressure gradient values are figured out for the pipeline systems by exposing to specified conditions such as roughness, temperature, rate of penetration, and their effects on the turbulence model behavior are also examined. Results obtained from the CFD simulations are validated with those of the flow-loop experiments conducted at both Izmir Katip Celebi University and Middle East Technical University. In general, CFD models give good agreement when compared with the previously published experimental data. The analysis leads to the following conclusions:

- For the water flow through the rough pipe, it can be observed that the RNG κ-ε model can be preferred reliably for estimating pressure losses.
- The analysis on the rough pipes allows the conclusion that the accuracy of the turbulence models slightly decreases as the pipe diameter increases from 80 mm to 90 mm and the relative roughness increases from 0.001 to 0.0013.
- For the water flow through the concentric annulus, EARSM and κ-ε models outperform the other turbulence models.
- For the water flow through the eccentric annulus, it is observed that all turbulence models give similar results that generally remain within the ± 20% percent error range. Although the RNG κ-ε model gives the optimum results for the low temperatures, it diverges from giving correct results as the temperature of the water increases.
- Besides, these findings provide additional information about the efficiency of the turbulence models predicting the pressure loss in the water flow through

the eccentric annulus. In almost all turbulence models, as the temperature increases, the efficiencies of the turbulence models decrease on a small scale.

- ω-Re turbulence model predicted pressure gradient better than other models at high fluid temperatures.
- For the sediment transport in the eccentric annulus, all turbulence models give similar results. However, the κ-ω and the ω-Re turbulence models give more appropriate results. This may be considered that the selection of ω based turbulence models is convenient for the sediment transport analysis.
- More generally, these basic findings demonstrate that it is possible to obtain satisfactory results with the selection of the right turbulence model.

REFERENCES

1. SORGUN, M. (2010). Modeling of Newtonian fluids and cuttings transport analysis in high inclination wellbores with pipe rotation.
2. SORGUN, M., ULKER,E. Friction factor calculation for turbulent flow in annulus with temperature effects. International Journal of Numerical Methods for Heat and Fluid Flow., 2020, 30.7: 3755-3763.
3. COTELA DALMAU, Jordi. Applications of turbulence modeling in civil engineering. 2016.
4. RODI, Wolfgang. Turbulence models and their application in hydraulics. CRC Press, 1993.
5. NICHOLS, Robert H. Turbulence models and their application to complex flows. University of Alabama at Birmingham, Revision, 2010, 4: 89.
6. FRIEDRICH, R., et al. Direct numerical simulation of incompressible turbulent flows. Computers & fluids, 2001, 30.5: 555-579.
7. MARKATOS, N. C. The mathematical modelling of turbulent flows. Applied Mathematical Modelling, 1986, 10.3: 190-220.
8. ANSYS Inc, (2009). CFX Solver Theory Guide. ANSYS Inc.
9. DURBIN, P.; SHIH, T. I. P. An overview of turbulence modeling. Modelling and Simulation of Turbulent Heat Transfer, 2005, 16: 3-31.
10. ARGYROPOULOS, C. D.; MARKATOS, N. C. Recent advances on the numerical modelling of turbulent flows. Applied Mathematical Modelling, 2015, 39.2: 693-732.
11. RODI, Wolfgang. Turbulence modeling and simulation in hydraulics: a historical review. Journal of Hydraulic Engineering, 2017, 143.5: 03117001.
12. TAYLOR, Robert P.; COLEMAN, Hugh W.; HODGE, B. K. Prediction of turbulent rough-wall skin friction using a discrete element approach. 1985.
13. HAGEN, Gotthlif Heinrich Ludwig. Über den einfluss der temperatur auf die bewegung des wassers in röhren--. Druckerei der Königl. akademie der wissenschaften, 1854.
14. DARCY, Henry. Recherches expérimentales relatives au mouvement de l'eau dans les tuyaux. Mallet-Bachelier, 1857.
15. JIMÉNEZ, Javier. Turbulent flows over rough walls. Annu. Rev. Fluid Mech., 2004, 36: 173-196.
16. NIKURADSE, Johann. Strömungsgesetze in rauhen Rohren. VDI-Verlag, 1933.
17. COLEBROOK, Cyril Frank. Turbulent flow in pipes, with particular reference to the transitional region between the smooth and rough wall laws. Journal of the Institution of Civil engineers, 1939, 11: 133-156.
18. MOODY, Lewis F. Friction factors for pipe flow. Trans. Asme, 1944, 66: 671-684.
19. LOUDA, Petr; PŘÍHODA, Jaromír; KOZEL, Karel. Numerical modelling of turbulent flow over rough walls. In: PAMM: Proceedings in Applied Mathematics and Mechanics. Berlin: WILEY-VCH Verlag, 2007. p. 4100011-4100012.
20. PERRY, Anthony Edward; SCHOFIELD, William H.; JOUBERT, Peter N. Rough wall turbulent boundary layers. Journal of Fluid Mechanics, 1969, 37.2: 383-413.
21. SHOCKLING, M. A.; ALLEN, J. J.; SMITS, A. J. Roughness effects in turbulent pipe flow. Journal of Fluid Mechanics, 2006, 564: 267-285.

22. TOWNSEND, A. A. The structure of Turbulent Shear Flow (Cambridge U. Press). 1976.
23. ALLEN, J. J., et al. Turbulent flow in smooth and rough pipes. Philosophical Transactions of the Royal Society A: Mathematical, Physical and Engineering Sciences, 2007, 365.1852: 699-714.
24. GIOIA, Gustavo; CHAKRABORTY, Pinaki. Turbulent friction in rough pipes and the energy spectrum of the phenomenological theory. Physical review letters, 2006, 96.4: 044502.
25. HULTMARK, Marcus, et al. Logarithmic scaling of turbulence in smooth-and rough-wall pipe flow. Journal of Fluid Mechanics, 2013, 728: 376-395.
26. PATEL, V. C. Perspective: flow at high Reynolds number and over rough surfaces—Achilles heel of CFD. 1998.
27. IBRAHIM, Mounir, et al. CFD Modeling of Surface Roughness in Laminar Flow. In: 2nd International Energy Conversion Engineering Conference. 2004. p. 5585.
28. HELLSTEN, Antti, et al. Extension of the k-omega-SST turbulence model for flows over rough surfaces. In: 22nd Atmospheric Flight Mechanics Conference. 1997. p. 3577.
29. VIJIAPURAPU, Sowjanya; CUI, Jie. Performance of turbulence models for flows through rough pipes. Applied Mathematical Modelling, 2010, 34.6: 1458-1466.
30. NOURMOHAMMADI, Khosrow; HOPKE, P. K.; STUKEL, J. J. Turbulent air flow over rough surfaces: II. turbulent flow parameters. 1985.
31. UNGER, F., FRIEDRICH, R. Large eddy simulation of fully-developed turbulent pipe flow. Eighth Symposium on Turbulent Shear Flows, 1991. p. 19-3.
32. ZAGAROLA, M. V.; SMITS, A. J. Scaling of the mean velocity profile for turbulent pipe flow. Physical review letters, 1997, 78.2: 239.
33. HUANG, K., et al. Experimental investigation on friction factor in pipes with large roughness. Experimental thermal and fluid science, 2013, 50: 147-153.
34. SZILAS, A. P.; BOBOK, E.; NAVRATIL, L. Determination of turbulent pressure loss of non-Newtonian oil flow in rough pipes. Rheologica Acta, 1981, 20.5: 487-496.
35. SHAIKH, Muhammad Mujtaba, et al. A new explicit approximation to Colebrook's friction factor in rough pipes under highly turbulent cases. International Journal of Heat and Mass Transfer, 2015, 88: 538-543.
36. BRKIĆ, Dejan. A note on explicit approximations to Colebrook's friction factor in rough pipes under highly turbulent cases. International Journal of Heat and Mass Transfer, 2016, 93: 513-515.
37. AVCI, A.; KARAGOZ, I. A new explicit friction factor formula for laminar, transition and turbulent flows in smooth and rough pipes. European Journal of Mechanics-B/Fluids, 2019, 78: 182-187.
38. WHITTAKER, Alun (ed.). Theory and application of drilling fluid hydraulics. International Human Resources Development Corporation, 1985.
39. DOSUNMU, Idowu T.; SHAH, Subhash N. Friction pressure prediction for annular flow of power law fluids. Chemical Engineering Communications, 2015, 202.10: 1380-1388.
40. LIU, Nan-Sheng; LU, Xi-Yun. Large eddy simulation of turbulent concentric annular channel flows. International journal for numerical methods in fluids, 2004, 45.12: 1317-1338.

41. ERGE, Oney, et al. Equivalent circulating density modeling of Yield Power Law fluids validated with CFD approach. Journal of Petroleum Science and Engineering, 2016, 140: 16-27.
42. SORGUN, MEHMET; OZBAYOGLU, M. E. Predicting frictional pressure loss during horizontal drilling for non-Newtonian fluids. Energy Sources, Part A: Recovery, Utilization, and Environmental Effects, 2011, 33.7: 631-640.
43. HACIISLAMOGLU, M.; LANGLINAIS, J. Non-Newtonian flow in eccentric annuli. 1990.
44. HACIISLAMOGLU, Mustafa, et al. Practical pressure loss predictions in realistic annular geometries. In: SPE Annual Technical Conference and Exhibition. Society of Petroleum Engineers, 1994.
45. KELESSIDIS, Vassilios C.; DALAMARINIS, Panagiotis; MAGLIONE, Roberto. Experimental study and predictions of pressure losses of fluids modeled as Herschel–Bulkley in concentric and eccentric annuli in laminar, transitional and turbulent flows. Journal of Petroleum Science and Engineering, 2011, 77.3-4: 305-312.
46. SORGUN, MEHMET. Computational fluid dynamics modeling of pipe eccentricity effect on flow characteristics of Newtonian and non-Newtonian fluids. Energy Sources, Part A: Recovery, Utilization, and Environmental Effects, 2011, 33.12: 1196-1208.
47. SAYINDLA, Sneha, et al. CFD Modeling of Hydraulic Behavior of Oil-and Water-Based Drilling Fluids in Laminar Flow. SPE Drilling & Completion, 2019.
48. UNER, Deniz; OZGEN, Canan; TOSUN, Ismail. An approximate solution for non-Newtonian flow in eccentric annuli. Industrial & engineering chemistry research, 1988, 27.4: 698-701.
49. LUO, Y.; PEDEN, J. M. Flow of non-Newtonian fluids through eccentric annuli, SPE Prod. 1990.
50. BRIGHTON, J. A.; JONES, J. B. Fully developed turbulent flow in annuli. 1964.
51. QUARMBY, Alan. An experimental study of turbulent flow through concentric annuli. International Journal of Mechanical Sciences, 1967, 9.4: 205-221.
52. REHME, K. Turbulent flow in smooth concentric annuli with small radius ratios. Journal of Fluid Mechanics, 1974, 64.2: 263-288.
53. LEVY, S. Turbulent flow in an annulus. 1967.
54. SINGH, R. P.; NIGAM, K. K.; MISHRA, P. Developing and fully developed turbulent flow through annuli. Journal of Chemical Engineering of Japan, 1980, 13.5: 349-353.
55. NOURI, J. M.; UMUR, H.; WHITELAW, J. H. Flow of Newtonian and non-Newtonian fluids in concentric and eccentric annuli. Journal of Fluid Mechanics, 1993, 253: 617-641.
56. SORGUN, Mehmet; OZBAYOGLU, M. Evren; AYDIN, Ismail. Modeling and experimental study of Newtonian fluid flow in annulus. Journal of Energy Resources Technology, 2010, 132.3.
57. XIONG, Xiao; AZIZ RAHMAN, Mohammad; ZHANG, Yan. RANS Based Computational Fluid Dynamics Simulation of Fully Developed Turbulent Newtonian Flow in Concentric Annuli. Journal of Fluids Engineering, 2016, 138.9.
58. GARDE, R. J. Sediment transport through pipes. CER; 56-19, 1956.
59. SINGH, Jatinder Pal; KUMAR, Satish; MOHAPATRA, S. K. Modelling of two phase solid-liquid flow in horizontal pipe using computational fluid dynamics technique. International journal of hydrogen energy, 2017, 42.31: 20133-20137.

60. KÖKPINAR, Mehmet Ali; GÖĞÜŞ, Mustafa. Critical flow velocity in slurry transporting horizontal pipelines. Journal of Hydraulic engineering, 2001, 127.9: 763-771.
61. LING, J., et al. Numerical investigations of liquid–solid slurry flows in a fully developed turbulent flow region. International Journal of Heat and Fluid Flow, 2003, 24.3: 389-398.
62. AMANNA, Behnam; MOVAGHAR, Mohammad Reza Khorsand. Cuttings transport behavior in directional drilling using computational fluid dynamics (CFD). Journal of Natural Gas Science and Engineering, 2016, 34: 670-679.
63. KAUSHAL, D. R., et al. CFD modeling for pipeline flow of fine particles at high concentration. International Journal of Multiphase Flow, 2012, 43: 85-100.
64. SHIRAZI, A. Sarraf; FRIGAARD, I. A. A three layer model for solids transport in pipes. Chemical Engineering Science, 2019, 205: 374-390.
65. SORGUN, Mehmet. Simple correlations and analysis of cuttings transport with newtonian and non-newtonian fluids in horizontal and deviated wells. Journal of Energy Resources Technology, 2013, 135.3.
66. TING, Xiong; MIEDEMA, Sape A.; XIUHAN, Chen. Comparative analysis between CFD model and DHLLDV model in fully-suspended slurry flow. Ocean Engineering, 2019, 181: 29-42.
67. LAHIRI, S. K.; GHANTA, K. C. Development of an artificial neural network correlation for prediction of hold-up of slurry transport in pipelines. chemical engineering science, 2008, 63.6: 1497-1509.
68. AZAMATHULLA, H. Md; AHMAD, Z. Estimation of critical velocity for slurry transport through pipeline using adaptive neuro-fuzzy interference system and gene-expression programming. Journal of Pipeline Systems Engineering and Practice, 2013, 4.2: 131-137.
69. ALIZADEHDAKHEL, Asghar, et al. CFD and artificial neural network modeling of two-phase flow pressure drop. International Communications in Heat and Mass Transfer, 2009, 36.8: 850-856.
70. ULKER, Erman; SORGUN, Mehmet. Comparison of computational intelligence models for cuttings transport in horizontal and deviated wells. Journal of Petroleum Science and Engineering, 2016, 146: 832-837.
71. CAPECELATRO, Jesse; DESJARDINS, Olivier. Eulerian–Lagrangian modeling of turbulent liquid–solid slurries in horizontal pipes. International journal of multiphase flow, 2013, 55: 64-79.
72. MESSA, Gianandrea Vittorio; MALAVASI, Stefano. Improvements in the numerical prediction of fully-suspended slurry flow in horizontal pipes. Powder Technology, 2015, 270: 358-367.
73. CAO, Deping; CHIEW, Yee-Meng. Suction effects on sediment transport in closed-conduit flows. Journal of Hydraulic Engineering, 2014, 140.5: 04014008.
74. AROLLA, Sunil K.; DESJARDINS, Olivier. Transport modeling of sedimenting particles in a turbulent pipe flow using Euler–Lagrange large eddy simulation. International Journal of Multiphase Flow, 2015, 75: 1-11.
75. ZHANG, Weijie, et al. Grouting Mechanism of Cement-Based Slurry in a Concentric Annulus under High Groundwater Pressure. Advances in Civil Engineering, 2019, 2019.

76. SORGUN, Mehmet. A mathematical model for estimating cuttings bed thickness in horizontal and deviated wells. International Journal of Oil, Gas and Coal Technology, 2017, 16.4: 329-341.
77. ESCUDIER, M. P. P. J., et al. Fully developed laminar flow of non-Newtonian liquids through annuli: comparison of numerical calculations with experiments. Experiments in fluids, 2002, 33.1: 101-111.
78. OZBAYOGLU, Mehmet Evren, et al. Effect of pipe rotation on hole cleaning for water-based drilling fluids in horizontal and deviated wells. In: IADC/SPE Asia Pacific Drilling Technology Conference and Exhibition. Society of Petroleum Engineers, 2008.
79. SORGUN, Mehmet; AYDIN, Ismail; OZBAYOGLU, M. Evren. Friction factors for hydraulic calculations considering presence of cuttings and pipe rotation in horizontal/highly-inclined wellbores. Journal of petroleum science and engineering, 2011, 78.2: 407-414.
80. GHASEMIKAFRUDI, E.; HASHEMABADI, S. H. Numerical study on cuttings transport in vertical wells with eccentric drillpipe. Journal of Petroleum Science and Engineering, 2016, 140: 85-96.
81. OFEI, Titus N.; IRAWAN, Sonny; PAO, William. Modelling of pressure drop in eccentric narrow horizontal annuli with the presence of cuttings and rotating drillpipe. International Journal of Oil, Gas and Coal Technology, 2015, 9.1: 39-60.
82. NETO, JL Vieira, et al. CFD applied to turbulent flows in concentric and eccentric annuli with inner shaft rotation. The Canadian Journal of Chemical Engineering, 2011, 89.4: 636-646.
83. NALLASAMY, M. A critical evaluation of various turbulence models as applied to internal fluid flows. National Aeronautics and Space Administration, Scientific and Technical Information Branch, 1985.
84. CFX-SOLVER, ANSYS. Theory guide. Release 12.1, 2009.
85. VAN WACHEM, B. G. M.; ALMSTEDT, Alf-Erik. Methods for multiphase computational fluid dynamics. Chemical Engineering Journal, 2003, 96.1-3: 81-98.
86. EESA, M.; BARIGOU, M. CFD investigation of the pipe transport of coarse solids in laminar power law fluids. Chemical Engineering Science, 2009, 64.2: 322-333.
87. ENWALD, Hans; PEIRANO, Eric; ALMSTEDT, A.-E. Eulerian two-phase flow theory applied to fluidization. International Journal of Multiphase Flow, 1996, 22: 21-66.
88. LAUNDER, Brian Edward; SPALDING, Dudley Brian. The numerical computation of turbulent flows. In: Numerical prediction of flow, heat transfer, turbulence and combustion. Pergamon, 1983. p. 96-116.
89. YAKHOT, VSASTBCG, et al. Development of turbulence models for shear flows by a double expansion technique. Physics of Fluids A: Fluid Dynamics, 1992, 4.7: 1510-1520.
90. WILCOX, David C. Formulation of the kw turbulence model revisited. AIAA journal, 2008, 46.11: 2823-2838.
91. MENTER, Florian R. Two-equation eddy-viscosity turbulence models for engineering applications. AIAA journal, 1994, 32.8: 1598-1605.

CURRIULUM VITAE

Personal Information:

Surname, Name: İlker, Pelin
Nationality: Turkish (TC)
Date and Place of Birth: 18 July 1989, İzmir
Marital Status: Married
Phone: + 90 532 557 57 78
e-mail: pelinilker@hotmail.com.tr

Education:

Degree	Institution	Year of Graduation
B.Sc.	Dokuz Eylul University Civil Engineering	2013
B.Sc.	Dokuz Eylul University Environmental Engineering (Double Major)	2013

List of Publications:

İlker, P., Sorgun, M. Performance Of Turbulence Models For Single Phase And Liquid-Solid Slurry Flows In Pressurized Pipe Systems. *Ocean Engineering*, 2020.

Conference Papers:

İlker, P., Sorgun, M. Numerical Simulation Of Water Flow In Annulus For Different Turbulent Models. International Civil Engineering and Architecture Conference, 2019,Trabzon, Turkey.

İlker, P., Sorgun, M. Numerical Modeling Of Sediment Transport In Closed Conduits", Internatıonal Symposium on Innovations in Civil Engineering and Technology Conference,2019, Afyon, Turkey.

Work Experience:

Year	Place	Enrollment
2018-	Izmir Katip Celebi University Civil Engineering	Research Assistant
2015-2016	Dorukkaya Mühendislik	Project Engineer